Volume 32
DOE/DP40200-63

LLE Review

Quarterly Report

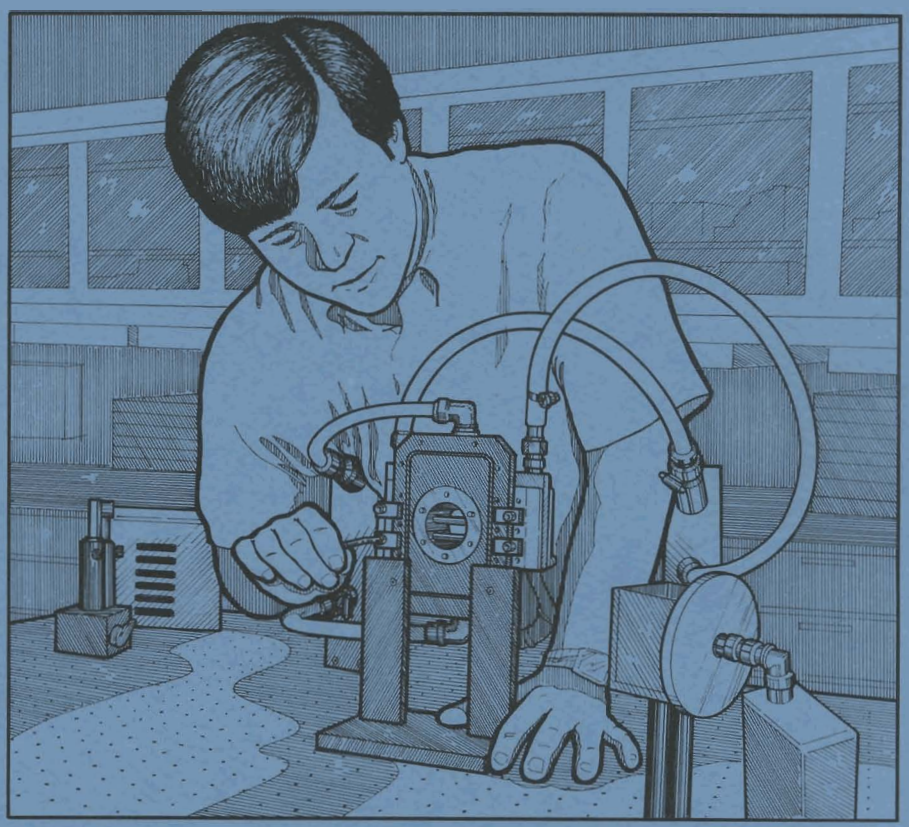

July–September 1987

Laboratory for Laser Energetics
College of Engineering and Applied Science
University of Rochester
250 East River Road
Rochester, New York 14623-1299

Volume 32
DOE/DP40200-63

LLE Review

Quarterly Report

Editor: W. Donaldson
(716) 275-5347

July–September 1987

Laboratory for Laser Energetics
College of Engineering and Applied Science
University of Rochester
250 East River Road
Rochester, New York 14623-1299

IN BRIEF

This volume of the LLE Review, covering the period July–September 1987, contains an article on the measurement of ρR in high-compression laser-fusion experiments using secondary reactions. The section on advanced technology has reports on the development of high-repetition-rate active-mirror amplifiers; electro-optic time-domain reflectometry; a new electro-optic finger probe; picosecond high-energy electron diffraction; and a method of using radial transmission lines to obtain very high electric fields. Finally, the activities of the National Laser Users Facility and the glass development and OMEGA laser facilities are summarized.

The highlights of this issue are

- A method for measuring the ρR in high-density laser-fusion experiments is described. The total ρR, the fuel ρR, and the mixing ratio can be determined from the ratio of two secondary reactions and the electron temperature.
- A 3.8-cm, clear-aperture Cr:Nd:GSGG active mirror has been designed and constructed. The small signal gain is 1.6 and the wave-front distortion is less than 3 waves at repetition rates of up to 10 Hz.
- Two articles describe electro-optic sampling. The first deals with a method that employs counterpropagating electric pulses to facilitate the acquisition of distortion-free electro-optic signals for time-

domain reflectometry. The second describes a new finger probe that uses total internal reflection of the optical probe.

- A new probe uses picosecond bursts of electrons to study the structure of surfaces. High-energy electrons reflect off the surface to give a time-resolved diffraction pattern. This is the first application of this technique to the picosecond time scale.
- An ultrafast high-voltage pulse injected into a radial transmission line exhibited a voltage gain of 2. This was the first experiment to demonstrate the feasibility of this concept for the construction of high-gradient, compact electron accelerators.

CONTENTS

David Smith, an engineer in the high-repetition-rate, solid-state sources group, has been responsible for a large part of the design and development of the Cr:Nd:GSGG active mirror, which he is shown adjusting. The high-repetition-rate sources group is currently developing slab and active-mirror geometry amplifiers in both glass and crystalline media.

Section 1
PROGRESS IN LASER FUSION

1.A ρR Measurements Using Secondary Reactions

A successful high-compression laser-fusion experiment is usually described in terms of achieving a satisfactory value of the density radius product ρR. Over the last several years, a number of techniques have been proposed to determine this product. Most of these techniques use the nuclear reaction products of the DT or DD reactions. One of the earliest proposals[1] to measure ρR noted that in DD reactions, one of the branches gives a triton at 1.06 MeV, which will have a finite probability of interacting with the deuterium fuel [^{3}H(D,n)^{4}He], giving rise to a high-energy neutron. The probability of this reaction occurring is proportional to the number of deuterons interacting with the triton in traversing the compressed fuel. It can be shown that this secondary reaction probability is proportional to the areal density ρR of the fuel. Blue[2] pointed out that the other branch of the DD reaction, which gives rise to a ^{3}He nucleus, would also undergo a secondary reaction ^{3}He(D,p)^{4}He, which gives a high-energy proton that can also escape from a highly compressed core. Since both the triton and the alpha particle are charged, they lose energy, in passing through the hot plasma. As the reaction products lose energy, the probability of a secondary reaction changes, since the interaction cross sections are strong functions of energy. The rate of energy loss is a function of the electron temperature of the plasma, which adds uncertainty to the interpretation of the measurements. Azechi *et al.*[3] pointed out that a simultaneous measurement of the fast-neutron and fast-proton production rates could give a measurement of both the effective electron temperature and the ρR of the compressed core.

Unfortunately, this answer is unique only if there is no mixing of the pusher with the fuel.

If mixing occurs before the time of neutron emission, the mass contributed by the pusher contributes to the slowing down of the reaction products but, naturally, cannot contribute directly to the production of secondary reactions. Thus, in the presence of mixing we have three unknowns: ρR, electron temperature, and mixing ratio. If simultaneous measurements can be made of the fast-neutron and fast-proton ratios with respect to the DD neutron production, and make an independent determination of the electron temperature, it is possible to determine the three unknowns.

For the purposes of this discussion, we will define the mixing ratio to be the fraction of the electrons in the compressed-fuel mixture that are contributed by the pusher material. If the pusher material has a Z/A equal to 1/2, then this definition gives the same value as what would be obtained by just using the mass ratio itself.

It is a straightforward procedure to calculate the expected ratio of the DT neutrons to the DD neutrons, and the ratio of the ^{3}He proton to the DD neutrons, for particular experimental conditions. A postprocessor has been added to the *LILAC* and *ORCHID* codes to make these predictions for specific simulations. An alternative approach is to assume a hot-spot emission model in which the DD reactions are produced in a very small region in the center of the fuel and the products proceed out radially through the rest of the fuel. The probability of producing the secondary reactions can be calculated as a function of the electron density, the electron temperature, the deuteron density, and the radius of the compressed core. In the situation of constant Z/A for all materials in the core, the product of electron density and core radius is linearly proportional to the total ρR of the fuel mixture. To calculate the energy loss in the plasma, we have used the expression given by Longmire[4]:

$$\frac{dE}{dX} = -\frac{N_e\, 4\sqrt{\pi}\, z_1^2 z_2^2 e^4\, \ln\Lambda\, m_1/m_2 \left[\int_0^{\alpha} e^{-y^2} dy - \left(1+\frac{m_2}{m_1}\right)\alpha e^{-\alpha^2}\right]}{E}, \quad (1)$$

where m_1 is mass of the fast particle; m_2 is mass of the electron; z_1 is charge of the fast particle; z_2 is charge of the electron;

$$\ln \Lambda = 24 - \ln\,(n_e{}^{0.5}/T_e)$$

is the coulomb logarithm; N_e is the electron density

$$\alpha^2 = \frac{m_2}{m_1} * \frac{E}{\kappa T}\ ;$$

and E = energy of the fast particle.

To carry out the computer calculation, the secondary triton is initiated at its energy of creation and propagated through a region of

constant electron and deuterium density. At each step, the energy loss to the triton and the probability that a $^3H(D,n)^4H$ reaction will occur is computed. This differential probability is equal to $N_D{*}s(E){*}\ Dx$. One then sums up the total probability for passing through a given mass of deuterium. These calculations are summarized in Fig. 32.1, which shows the predicted ratios of DT neutrons to DD neutrons as a function of ρR in gm/cm^2, with the electron temperature as a parameter. These curves assume no mixing, i.e., the electron density is equal to the deuterium density. Figure 32.2 shows the results for the ^3He proton production. It is interesting to note the difference between the two sets of curves. The fast-proton ratio curves are smooth, with the first derivative always falling. This results from the fact that the peak in the cross section of the ^3He-D reaction occurs at a larger energy than the 0.8-MeV maximum in this experiment. Also note that the ^3He particles have a relatively short range in the plasma and thus, for moderately large ρR – i.e., values greater than 10 mg/cm^2 – the proton/neutron ratios are more sensitive to the temperature than to ρR. The tritons, being charge one, have a much larger range than the ^3He particles; thus, the fast- to slow-neutron ratios depend on both the temperature and the ρR. The peak of the triton reaction occurs at much lower energy than the 1.06 MeV the triton is born with. This leads to an increase in the slope of the probability curves near the end of the triton range. In the absence of mixing, the two measurements together give a unique prediction for the fuel temperature and the ρR.

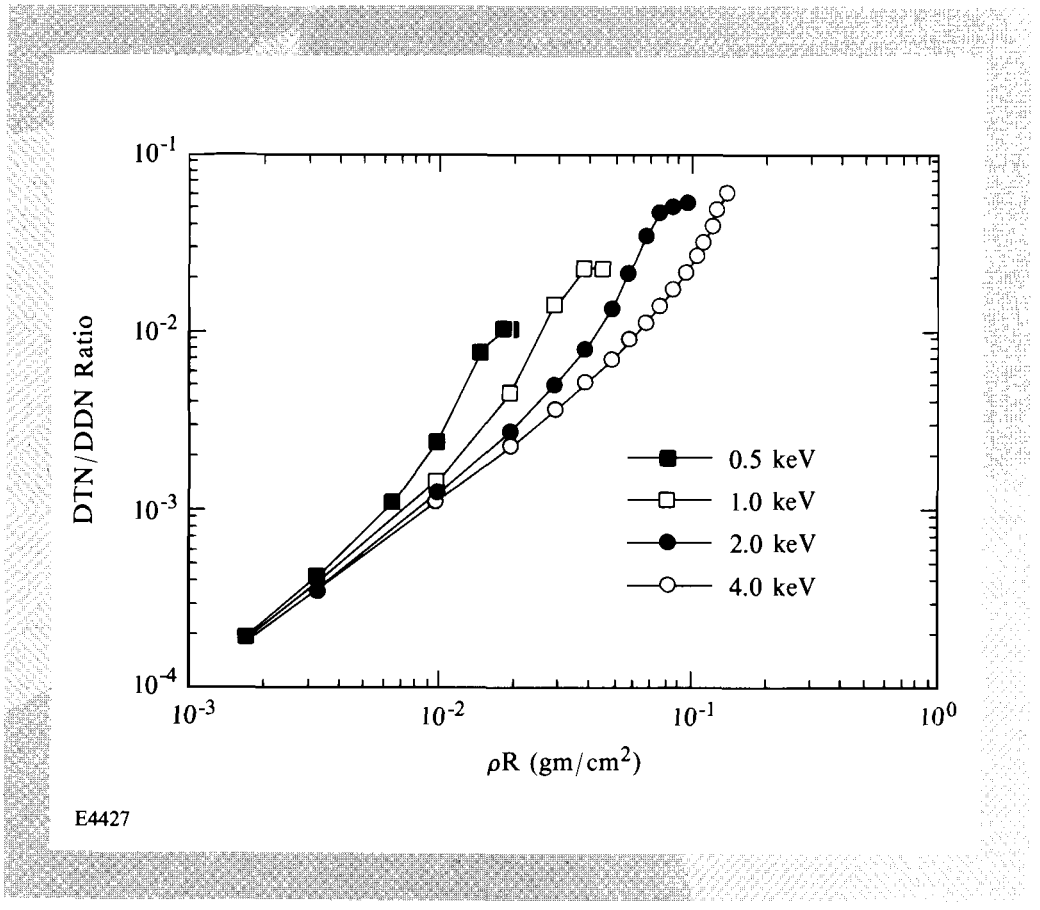

Fig. 32.1
Calculated probability of the production of fast neutrons from the $^3H(D,n)^4He$ reaction versus ρR (gm/cm^2), with electron temperature as the parameter. These calculations assume a hot-spot model, i.e., that all the DD neutrons are produced near the center of the compressed core.

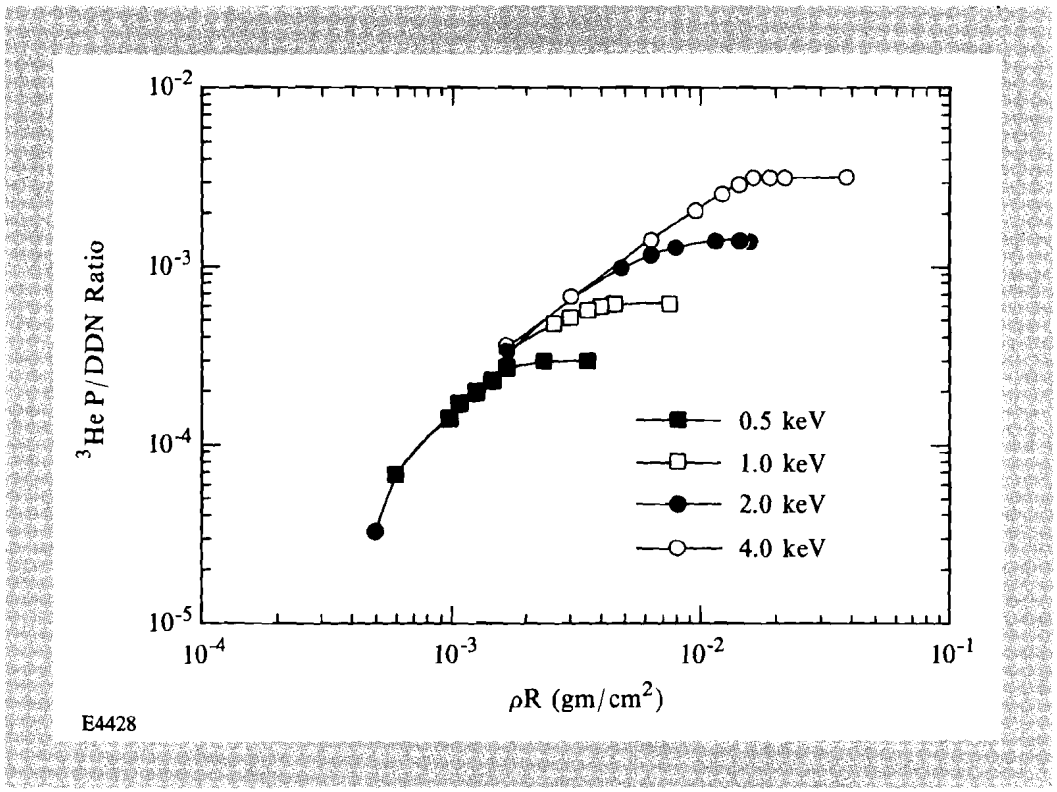

Fig. 32.2
Calculated probability of production of fast protons from the ^{3}He(D,p)^{4}He reaction, with electron temperature as the parameter.

In the presence of mixing, an independent measurement or estimate of the core electron temperature is needed. The effect of mixing is to change the ratio of electron density to deuteron density. The effect on the ^{3}He secondaries is simple, i.e., the range of the fast particle is determined by the total $(\rho R)_T$; however, the secondary probability is given by the $(\rho R)_F$, which is the areal mass of the deuterium alone. It was noted earlier that the ^{3}He(D,p)^{4}He peaks at the highest energy; thus, the extra stopping power of the high-Z mixed materials can only reduce the number of secondaries. The situation for the tritons' reactions is more complicated because the peak of the cross section occurs at relatively low energy. For the experiments of current interest, in which the expected electron temperature is less than 3 keV, the fast-proton measurement will determine a mixing ratio almost independent of the fast-neutron result, provided the total ρR is greater than 5 mg/cm^3. This becomes clearer if we take a hypothetical experimental result.

Assume that a simulation predicts that the nonburning fuel should be at 0.5 keV and a proton/DD neutron ratio of 1.0×10^{-4} and a DTN/DDN ratio of 2.1×10^{-3} are observed. The predicted proton ratio at 0.5 keV is 3.0 for a ρR greater than 3 mg/cm^2. It can therefore be concluded that the mixing ratio = predicted/measured proton value was 3 for this illustration. Returning to the fast-neutron measurements, we note that the number of fast neutrons would have been three times larger if the tritons had passed through deuterium alone. We therefore look up the effective $(\rho R)_T$ by looking up the predicted value at a ratio of $3 \times 2 \times 10^{-3}$, which for this case is 13.7 mg/cm^2. The deuterium $(\rho R)_F$ is equal to 13.7/3 = 4.6 mg/cm^2.

This analysis makes no assumptions about the total ρR, and thus is independent of the simulations except possibly for estimating the electron temperature. In summary, the total ρR, the fuel ρR, and the mix ratio can be deduced from the knowledge of the two secondary ratios and the electron temperature.

A note concerning the laboratory measurements of the secondary ratios: For many of the experiments on OMEGA, the number of secondary reactions is small; therefore, detectors with large solid angles are required. Currently, we are using plastic scintillators with a 1×10^{-3} fractional solid angle to detect the fast neutrons, and CR-39 solid-state detectors with a $>1 \times 10^{-2}$ fractional solid angle to detect the 14.7-MeV protons.

ACKNOWLEDGMENT

This work was supported by the U.S. Department of Energy Office of Inertial Fusion under agreement No. DE-FC08-85DP40200, and by the Laser Fusion Feasibility Project at the Laboratory for Laser Energetics, which has the following sponsors: Empire State Electric Energy Research Corporation, General Electric Company, New York State Energy Research and Development Authority, Ontario Hydro, and the University of Rochester. Such support does not imply endorsement of the content by any of the above parties.

REFERENCES

1. E. G. Gamali *et al.*, *JETP Lett.* **21**, 70 (1975).
2. T. E. Blue and D. B. Harris, *Nucl. Sci. Eng.* **77**, 463 (1981).
3. H. Azechi *et al.*, *Appl. Phys. Lett.* **49**, 555 (1986).
4. C. Longmire, *Elementary Plasma Physics* (Wiley, New York, 1963), pp. 196–197.

Section 2
ADVANCED TECHNOLOGY DEVELOPMENTS

2.A A High-Repetition-Rate, Cr:Nd:GSGG Active-Mirror Amplifier

The active-mirror geometry amplifier was invented at General Electric[1] and developed at LLE in a program[2] that culminated in the deployment of a Nd:glass-active-mirror final-amplifier stage on the single-beam glass development laser (GDL) system.[3] These four 21-cm clear-aperture units produced 660 J in an 0.8-ns pulse[3] in single-shot operation. In the past year, a program has begun to develop the active-mirror geometry amplifier as a high-repetition-rate device.[4] This article describes the first results of that program.

A high-repetition-rate active mirror is shown schematically in Fig. 32.3. The mirror consists of a circular plate of the gain medium, cooled and pumped from one side by a length-tailored array of flash lamps. Key to the operation of the active mirror are the dielectric thin-film coatings applied to the plate. The coating on the rear (pumped) side of the plate is highly reflecting at the gain wavelength and highly transmitting at the pump wavelength. The front coating is the converse of the rear – highly antireflecting at the gain wavelength and highly reflecting at the pump wavelength. In operation, both the beam to be amplified and the pump light double pass the gain medium for efficient extraction and absorption. Cooling is done through a major face only, to ensure that with uniform pumping thermal gradients are parallel to the direction of propagation of the amplified beam. It is possible to simultaneously cool both major faces if a suitably transmissive coolant for the front can be identified. The circumference of the plate is angled and fine ground to defeat parasitic oscillation and reduce amplified

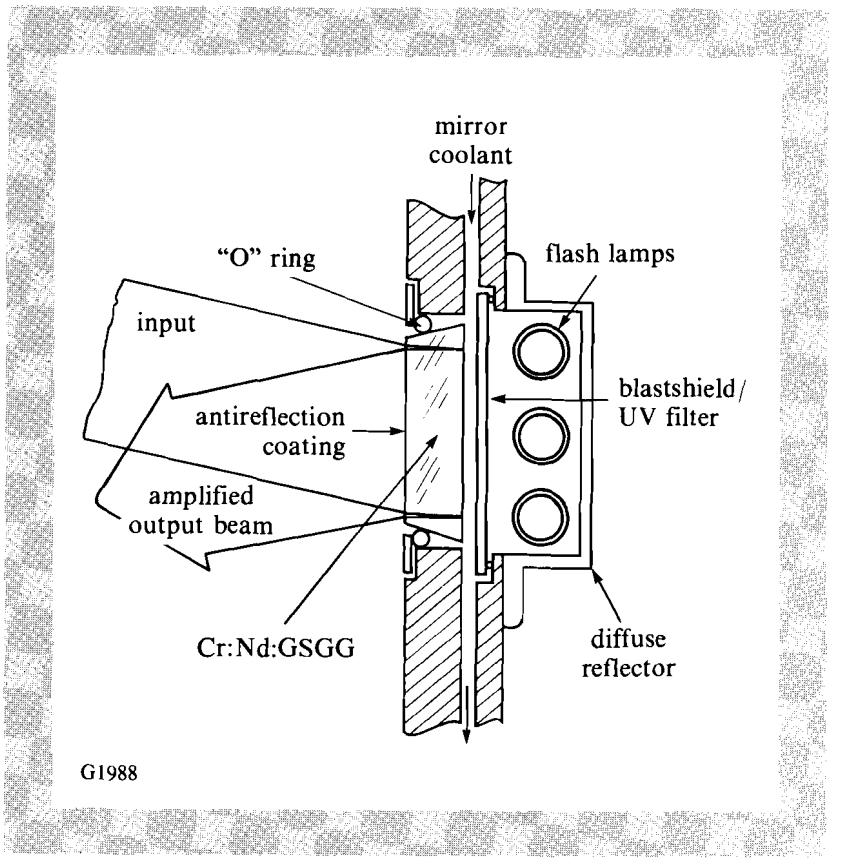

Fig. 32.3
High-repetition-rate active-mirror technology.

spontaneous emission (ASE) losses. The front and rear of the mirror are at a slight angle to deflect residual front-face reflections out of the amplified beam and to further discriminate against parasitics. A combination blast shield and UV filter protects the active medium from ultraviolet light emitted by the flash-lamp array.

The active-mirror geometry amplifier is a very attractive high-repetition-rate device from a number of standpoints. As already mentioned, propagation is parallel to thermal gradients, thereby eliminating dn/dT focusing when uniformly pumped. The active mirror is inherently double passed for both the laser and pump light. Compared to Brewster angle slabs, fabrication of the round plate is simple, which leads to lower costs. The clear aperture is round, eliminating the need for anamorphic transport optics. Finally, for a given clear aperture, the active-mirror geometry offers the shortest possible major dimension, thereby minimizing ASE difficulties. In order to enjoy these advantages of the active-mirror geometry, the moderate-gain path length and the thermal bending of the plate must be understood.

The co-doped crystalline material Cr^{+3}:Nd^{+3}:GSGG was chosen as the active medium. It offers a much higher effective stimulated emission cross section,[5] $\sigma(^4F_{3/2}-^4I_{11/2}) = 1.3 \times 10^{-19}$ cm^2, compared to that of the LHG-8 glass[6] used in the large active mirrors,[7] $\sigma = 4.0 \times 10^{-20}$ cm^2. This implies a higher small-signal gain per unit inversion. Co-doped GSGG was available in large core-

free boules with diameters of 4 cm at the time of acquisition (April 1986). It is thermally and optically isotropic when unstressed. The co-doping and effective energy transfer[8] from the Cr^{+3} to the Nd^{+3} increases pump absorption and reduces the very high pump powers needed with purely Nd^{+3}-doped crystals. GSGG has a high thermal conductivity characteristic of crystals, a large Young's modulus, and high fracture stress limit, which are summarized by the thermal stress resistance parameter R_S.[9] The R_S of GSGG[5] of 6.6 W/cm is half that of Nd:YAG but still over six times that of the LHG-5 glass.[6] Finally, for the active-mirror application, this material is readily coated with dielectric thin films.

The GSGG active mirror is 4.0 cm in diameter, with a 3.8-cm clear aperture defined by the coatings. The thickness was chosen to be 0.95 cm for purely mechanical reasons. This thickness allows mounting by a circumferential O-ring without deformation of the plate. The plate itself was cut from the boule, perpendicular to the boule's axis. The Cr^{+3} and Nd^{+3} dopings were 1 and 2 $\times$ 10^{20} ions/cc, respectively. These are vendor-supplied numbers.[10] The absorption through the plate at the peak of the Cr^{+3} 460-nm absorption band is in excess of OD 4. Although determining the optimum doping levels is a complex problem, requiring the balancing of absorption, plate thickness, Cr^{+3} to Nd^{+3} energy transfer, and concentration quenching, it is clear that these dopings, dictated by material availability, were high for the chosen plate thickness.

The GSGG plate was measured interferometrically prior to coating for transmitted wave-front quality. The transmitted wave front at 1 μm was less than 1/3 wave, peak to valley. This 1/3 wave was subsequently determined, by surface interferometry, to be almost entirely due to the edge rolloff characteristic of the polished material. There was also some high-frequency ($\sim$ 1-mm), very low contrast structure on the transmission interferograms. The source of this structure has not been determined.

The spatially resolved birefringence of the plate was measured at 632.8 nm, using a scanning-modulated transmission ellipsometer.[11] The plate was scanned across a diameter, using a 2-mm beam. The birefringence typically started at 0.7 nm/cm in the center of the plate, increased slightly to $\sim$1 nm/cm at a radius of 1 cm, and then decreased through zero to a value of $\sim$ -2 nm/cm at the edge of the plate. The circumference of the plate is initially in compression.

The fluorescence lifetime (1/e) of the Nd^{+3} was measured to be 280 ± 17 μs, using a standard apparatus in use at LLE for measuring Nd in glass lifetimes.

The plate is pumped by a shape-tailored array of three, 8-mm bore, 300-Torr xenon flash lamps. The top and bottom lamps (see Fig. 32.3) have a 1.5-in. arc length, and the middle lamp has a 2.0-in. arc length. The lamps are driven with a 300-μs, 1/3-current maximum-full-width, critically damped pulse. The maximum single-pulse energy is 460 J. A switch mode charger[12] provided 4 kW of power for the lamps. At

maximum bank energy, the peak repetition rate was 8.7 Hz; operation at 10 Hz was obtained by reducing the bank energy to 400 J. The lamps are mounted in a common flooded cavity.

The active-mirror head itself is modular in design. A single plate and compression ring hold the mounting O-ring for the GSGG. A 0.125-in. spacer plate defines the cooling channel. The active mirror is cooled with a 50/50 mixture of ethylene glycol and water. Typical flow rates are ~4 gal per minute. The flash-lamp array, UV filter, and blast shield assembly bolt over the coolant plate. The UV filter is a Schott[13] WG-320, 320-nm UV cutoff filter. The cutoff wavelength was chosen to be between the ~300-nm GSGG UV edge and the 346-nm Nd^{+3} absorption band.

The small signal gain was measured at the center of the active mirror as a function of bank energy. The probe beam was from a Q-switched GSGG oscillator with a pulse width of 0.5 μs, and was attenuated to ensure that the small signal gain was being measured. The measured gain did not change within the error bars when the input intensity was changed by a factor of 10 (i.e., an ND = 1.0 inserted into the beam). The gain was measured using the ratio of ratios technique,[14] which eliminates any errors due to probe fluctuations. Figure 32.4 shows the gain as a function of bank energy. The maximum gain measured was 1.61 ± 0.04. Overlaid with the data is a simulation of the expected small signal gain from the code TRENDE.[15] This code takes into account the time and wavelength dependence of the flash-lamp emission and the active material absorption spectrum. The simulation shown in Fig. 32.4 did not

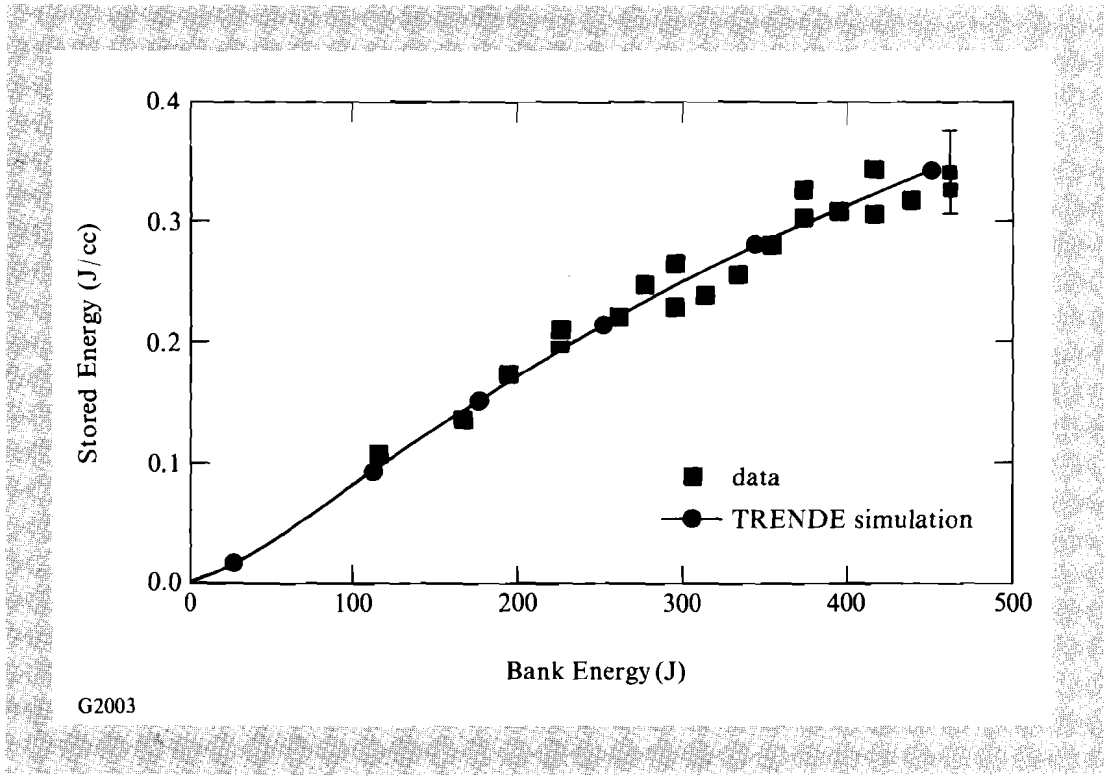

Fig. 32.4
Small signal gain versus bank energy, in joules.

invoke any ASE losses. Good agreement of the code with the experiment indicates that the device is not limited by ASE. The slight curvature that is seen in both the simulation and the data comes from the fact that as the flash lamps are driven harder, the pump spectrum shifts slightly to shorter wavelengths. TRENDE also calculates the inversion as a function of mirror thickness. By multiplying by the χ factor,[16] the inversion may be converted to heat deposition as a function of thickness.

Knowledge of both the stimulated emission cross section and the small signal gain allows calculation of the stored energy density in the mirror. Using a cross section of 1.3×10^{-19} cm^2, and a gain of 1.61, yields an average stored energy of 0.361 J/cm^3. If we multiply this value by the volume of the active mirror, we obtain the total energy stored in the upper lasing level that is accessible, assuming uniform pumping. This value has been calculated to be 3.9 J. If we assume an 80% fill factor and that we extract 75% of the energy, the total energy that can be added to a laser beam is found to be 2.3 J for this mirror. At a repetition rate of 8.7 Hz, this represents an average extractable power of 20 W.

The gain uniformity was measured by imaging the fluorescence of the mirror onto a CID camera.[17] The camera was placed approximately 40 cm away from the mirror to ensure that no vignetting of the image in the camera's lens system occurred, and it was double filtered with a three-cavity interference filter and an RG 1000 long-pass filter to guarantee that no pump light would reach it. The fluorescence was found to be parabolic in profile with the edge at 80% of the level at the center of the mirror.

Lateral-shearing interferometry[18] was performed on both a beam reflected from the front surface of the mirror and a beam passing the mirror material and reflecting from the rear surface. The front surface was sheared with a frequency-doubled YAG, which was reflected by the front surface coating. The total wave front was sheared with the same YAG without doubling. The slight wavelength difference between Nd:YAG at 1.064 μm and Nd:GSGG at 1.061 μm eliminated gain effects. Data was taken as a function of average pump power and recorded with a CID camera connected to a video cassette recorder. Lateral-shearing interferograms may be readily interpreted to yield the waves of defocus on the sheared beam in one dimension.[18] Interferograms were taken in both the horizontal and vertical directions and were found to be equal to within the error bars of the experiment (± 0.25 μm).

Thin-plate theory[19] predicts purely parabolic and equal (within a constant) surface displacements of a traction-free plate with a temperature variation through its thickness only. The thin-plate approximation is not valid in regions that are within one plate thickness of an edge. Because the thickness of the Cr:Nd:GSGG places a large fraction of the mirror near the edge, a finite-element code CYLLAS was written to predict the surface displacements. This code uses as input the thermomechanical properties of Cr:Nd:GSGG and the

TRENDE-computed energy deposition rate as a function of thickness. It solves the steady-state, Fourier heat conduction equation in one dimension, with the boundary condition that the front face is insulated and that the cooling of the rear surface may be approximated with a film coefficient. The computed temperature profile is then used to calculate the stresses, strains, and displacements. Once the displacements are known, a ray trace of the mirror is performed to determine the optical path difference (OPD) between center and edge.

Figure 32.5 shows the measured front surface displacement at the edge of the aperture due to defocus. Also shown on this figure is the CYLLAS-predicted displacement for a χ value of 2.0. Note the close agreement.

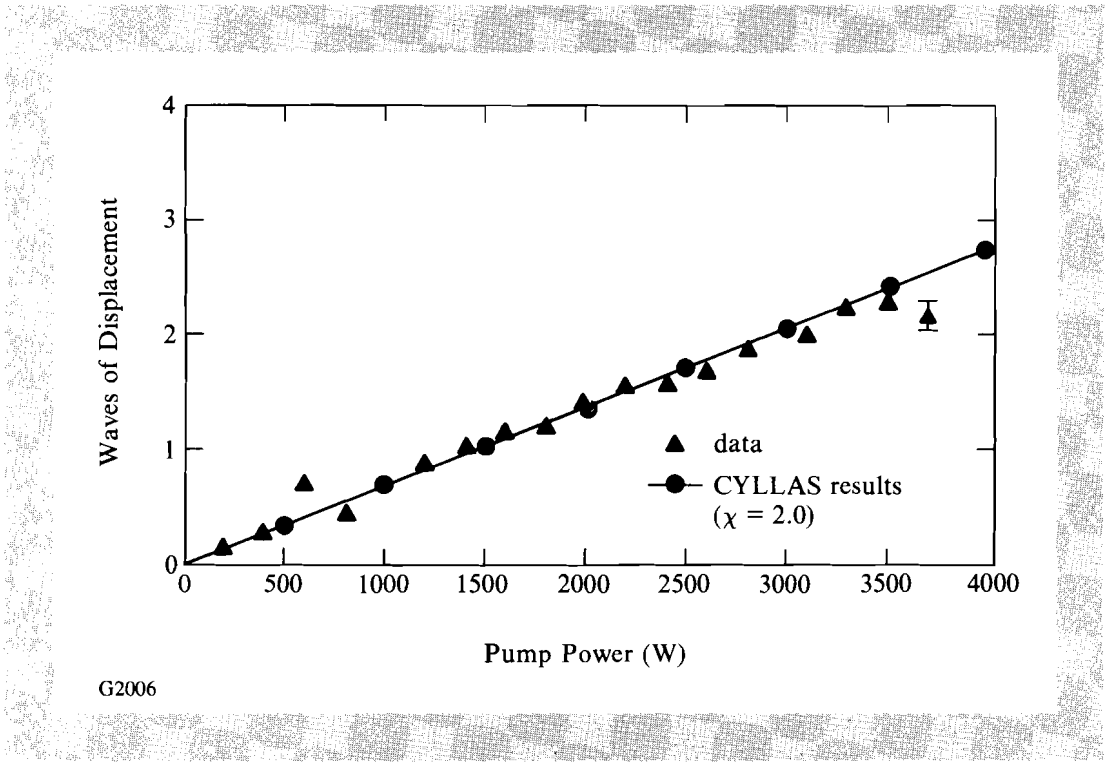

Fig. 32.5
Front surface edge displacement in waves at 1.06 μm versus average pump power in watts.

Figure 32.6 is a plot of the number of waves of defocus at the edge of the aperture on the beam reflected from the back surface versus pump power. Also plotted are the predictions of the code CYLLAS for two cases. In the first case, the mirror is assumed uniformly pumped and ~ 5 waves of defocus are predicted at maximum power. In the second case, a parabolic radial temperature profile with the edge of the mirror at 90% of the center temperature was assumed. In this second case, dn/dT^{20} was included in the OPD calculation and good agreement with the measured ~ 3 waves was obtained. While the steady-state bending of the mirror causes it to act as a negative lens, this is partially compensated for by the GSGG itself acting as a positive lens. The difference between the 20% center-to-edge decline in fluorescence and the inferred 10% center-to-edge decline in temperature is hypothesized to be due to radial direction heat conduction.

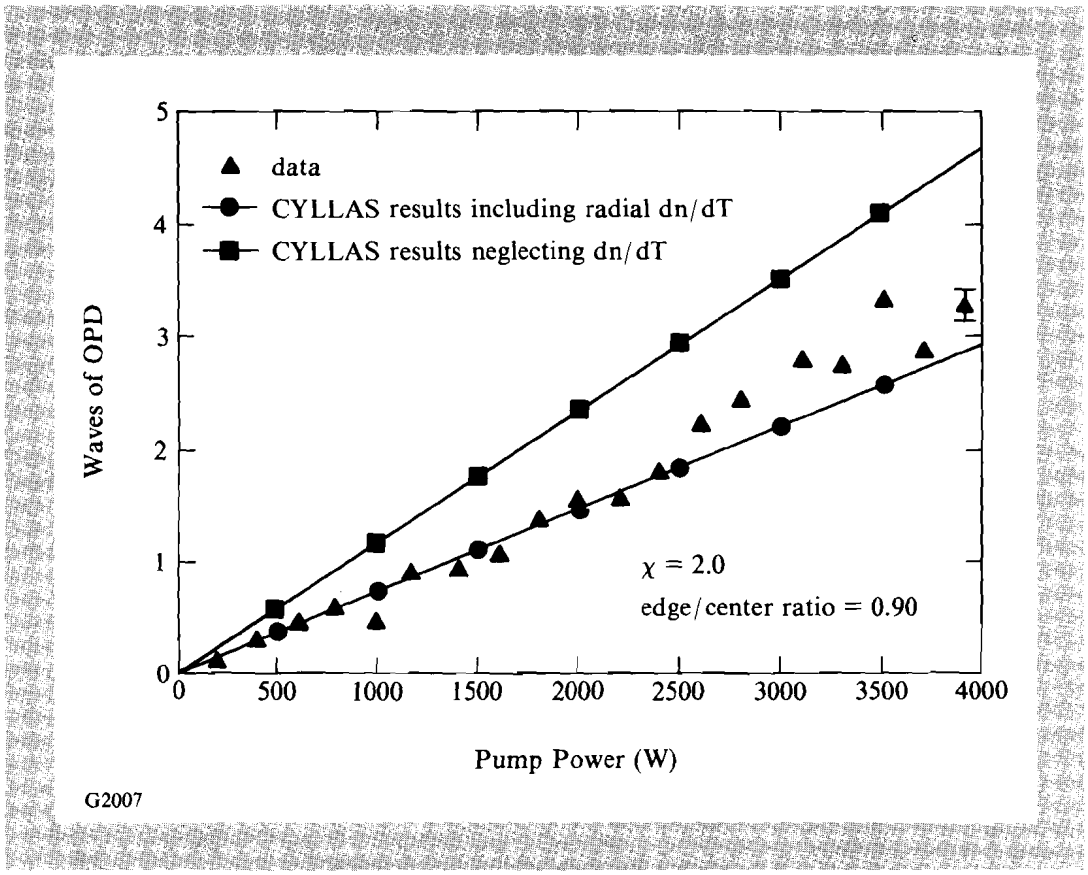

Fig. 32.6
Center-to-edge optical path difference in waves at 1.06 μm versus average pump power in watts.

As the mirror's pump power is increased, CYLLAS predicts that the circumference ($\sigma_{\theta\theta}$) will go into tension after overcoming the initial compression. The consequent stress-induced birefringence was probed by placing the mirror between crossed polarizers and measuring the transmission with a small beam, with the input polarizer at 45° to a radius. At the edge of the clear aperture, the transmission was 2.4% when unpumped, went down below 0.5% at 2-kW pump power, and then increased to 2.5% at full (4-kW) pump power. The 2.5% depolarization at the edge was the maximum observed in the clear aperture.

In conclusion, we have demonstrated the highest-repetition-rate (10-Hz) and highest-gain (1.6) active mirror published to date. This device is also the largest clear-aperture (3.8-cm) Cr:Nd:GSGG amplifier yet reported. Measurements of gain and wave front show good agreement with the theoretical models. New designs are being pursued for a next-generation, high-repetition-rate active mirror that will improve small signal gain, repetition rate, and wave-front quality.

ACKNOWLEDGMENT

This work is supported by Daewoo Heavy Industries of Incheon, Korea. The authors gratefully acknowledge the technical assistance of M. Tedrow and J. Suhan through all phases of the experiment.

REFERENCES

1. J. P. Chernoch, U. S. Patent No. 3 466 569 (9 September 1969).
2. J. A. Abate, L. Lund, D. Brown, S. Jacobs, S. Refermat, J. Kelly, M. Gavin, J. Waldbillig, and O. Lewis, *Appl. Opt.* **20**, 351 (1981).
3. T. Kessler, W. Seka, J. Kelly, D. Smith, R. Bahr, W. Lockman, N. Wong, and J. Soures, *High-Power and Solid-State Lasers* (SPIE, Bellingham, WA, 1986), Vol. 622, p. 156.
4. D. C. Brown, R. Bowman, J. Kuper, K. K. Lee, and J. Menders, *Appl. Opt.* **25**, 612 (1986).
5. W. F. Krupke *et al.*, *J. Opt. Soc. Amer. B* **3**, 102 (1986).
6. Product of Hoya Optics, Inc., 3400 Edison Way, Fremont, CA 94538.
7. S. E. Stokowski, R. A. Saroyan, and M. J. Weber, "Nd-Doped Laser Glass Spectroscopic and Physical Properties," prepared at Lawrence Livermore Laboratory under contract W-7405-Eng-48, 1978.
8. D. Pruss, G. Huber, and A. Beimowski, *App. Phys. B* **28**, 355 (1982).
9. J. M. Eggleston *et al.*, *IEEE J. Quantum Electron.* **QE-20**, 289 (1984).
10. Airtron, 200 E. Hanover Ave., Morris Plains, NJ 07950.
11. S. D. Jacobs, J. E. Hayden, and A. L. Hrycin, *Optical Thin Films II: New Developments* (SPIE, Bellingham, WA, 1986), Vol. 678, p. 66.
12. A. L. E. Systems model 302L, A. L. E. Systems Inc., 150 Homer Avenue, Ashland, MA 01721.
13. Schott Glass Technologies Inc., 400 York Avenue, Duryea, PA 18642.
14. J. V. Meier, N. P. Barnes, D. K. Remelius, and M. R. Kokta, *IEEE J. Quantum Electron.* **QE-22**, 2058 (1986).
15. J. H. Kelly, Ph. D. thesis, University of Rochester, 1980, available from University Microfilms International, Ann Arbor, MI 48106.
16. M. S. Mangir and D. A. Rockwell, *IEEE J. Quantum Electron.* **QE-22**, 574 (1986).
17. General Electric model 2505-A3, G. E. Co., 890 7th St. North, Liverpool, NY 13088.
18. D. Malacara, *Optical Shop Testing* (Wiley, New York, 1978), p. 105.
19. B. A. Boley and J. H. Weiner, *Theory of Thermal Stresses* (Wiley, New York, 1960).
20. J. C. Lee and S. D. Jacobs, *Appl. Opt.* **26**, 777 (1987).

2.B Counterpropagating Pulses for Ultrahigh-Frequency Electro-Optic Time-Domain Reflectometry

In recent years, the achievable-gain bandwidth product for solid-state devices has increased to the point where electronic time-domain reflectometers (TDR) and network analyzers are often unsuitable for device characterization. The bandwidth limitations of conventional instrumentation can be largely attributed to the electrical parasitics associated with probes, which require mechanical contact with the device to be tested. As a consequence, much recent research has been devoted to noncontact characterization based on picosecond optical pulses.[1-3] Prominent among this class of methods is electro-optic sampling, which typically employs a stable, high-repetition-rate (approximately 100-MHz), picosecond laser combined with conventional electronic-signal-processing methods.[3] This approach permits the direct observation of electrical signals on electro-optic substrates such as GaAs[4] or through noninvasive finger probing at virtually any location in a substrate-independent fashion.[5] (See the article, "A Substrate-Independent Noncontact Electro-Optic Probe Using Total Internal Reflection," in this issue.) Here we propose a new method of time-domain reflectometry based on the electro-optic sampling technique and the principle of counterpropagating pulses, and present experimental results of symmetrical pulse generation.

In general, the TDR consists of a step or impulse signal source and a feedthrough waveform acquisition instrument connected to the device under test (DUT), as shown in Fig. 32.7. An electrical waveform propagates from the pulse generator to the DUT, and the acquisition instrument detects the waveforms incident upon and reflected from the DUT input for subsequent analysis. It is desirable to locate the plane of observation of the sampling instrument at the DUT/transmission line interface to minimize distortion; however, the resulting temporal overlap of the incident and reflected waveforms makes it impossible to observe the DUT behavior. The observation plane must therefore be separated from the device input; several problems, however, that are especially severe for physically small, high-bandwidth DUT's then arise. For example, the measured waveforms differ from the true-

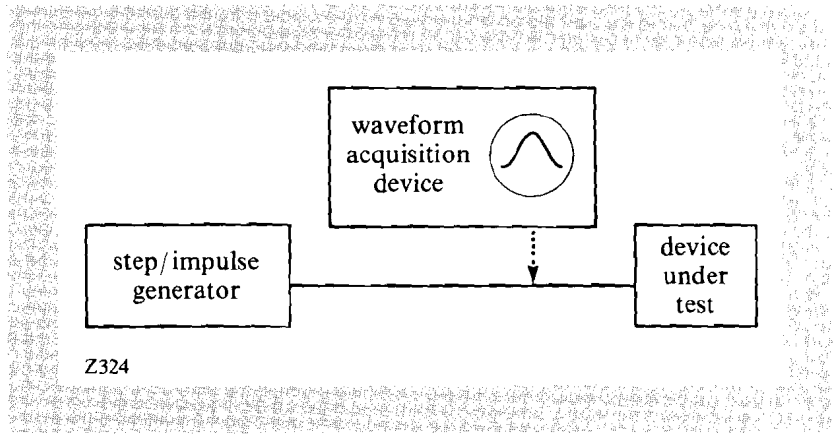

Fig. 32.7
Time-domain reflectometer.

incident and reflected waveforms due to dispersion and frequency-dependent attenuation caused by the section of transmission line between the DUT input and the waveform acquisition instrument. The effect of wafer probes, connectors, attenuators, or other waveform-distorting elements that lie in the signal path must also be de-embedded from the data. It is these problems we address with the symmetrical pulse propagation technique.

In one implementation of this concept, a coplanar waveguide and a photoconductive switch were fabricated, using a liftoff process on 1500 Å of thermally evaporated nickel-gold-germanium on a semi-insulating <100>-cut GaAs substrate. The lines were 3 cm in length, with the switch positioned 1 cm from one end of the waveguide, as pictured schematically in Fig. 32.8. A photomicrograph of the switch detail is shown in Fig. 32.9.

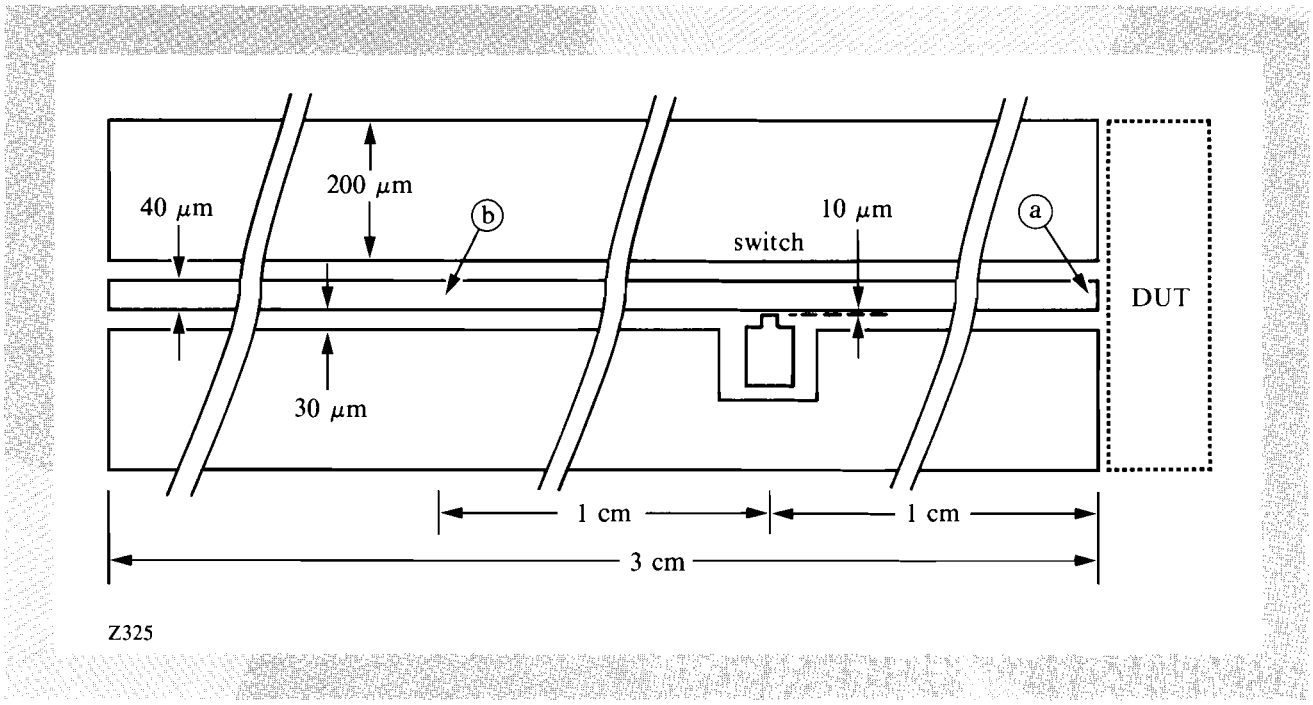

Fig. 32.8
Waveguide detail.

A compressed picosecond optical pulse from a frequency-doubled YAG laser (λ = 532 nm) was focused onto the 10-μm switch gap, which was biased with a 100-kHz sine wave. The resulting optically generated carriers in the gap produced an electrical transient on the central waveguide conductor that propagated away from the switch in both directions on the waveguide.

As the symmetrically propagating pulses travel on the waveguide, they undergo equal degrees of attenuation and dispersion per unit distance. Therefore, the waveform that arrives at point (b) in Fig. 32.8 will appear identical to the waveform arriving at point (a), and by electro-optically sampling the waveform at point (b), the waveform incident on the DUT is predicted. The reflected waveform is then obtained by subtracting the incident waveform from the waveform obtained at point (a).

Z335

Fig. 32.9
Switch detail.

The electro-optic sampling was realized using a sub-bandgap (λ = 1.06 μm) laser pulse to probe the electric field emanating from the central conductor of the waveguide. The signal was then processed by a signal averager and lock-in amplifier. Since the excitation and sampling laser pulses originated from the same source, they were precisely synchronized, yielding jitter-free waveform acquisition.[3] A schematic of the electro-optic sampling system is shown in Fig. 32.10.

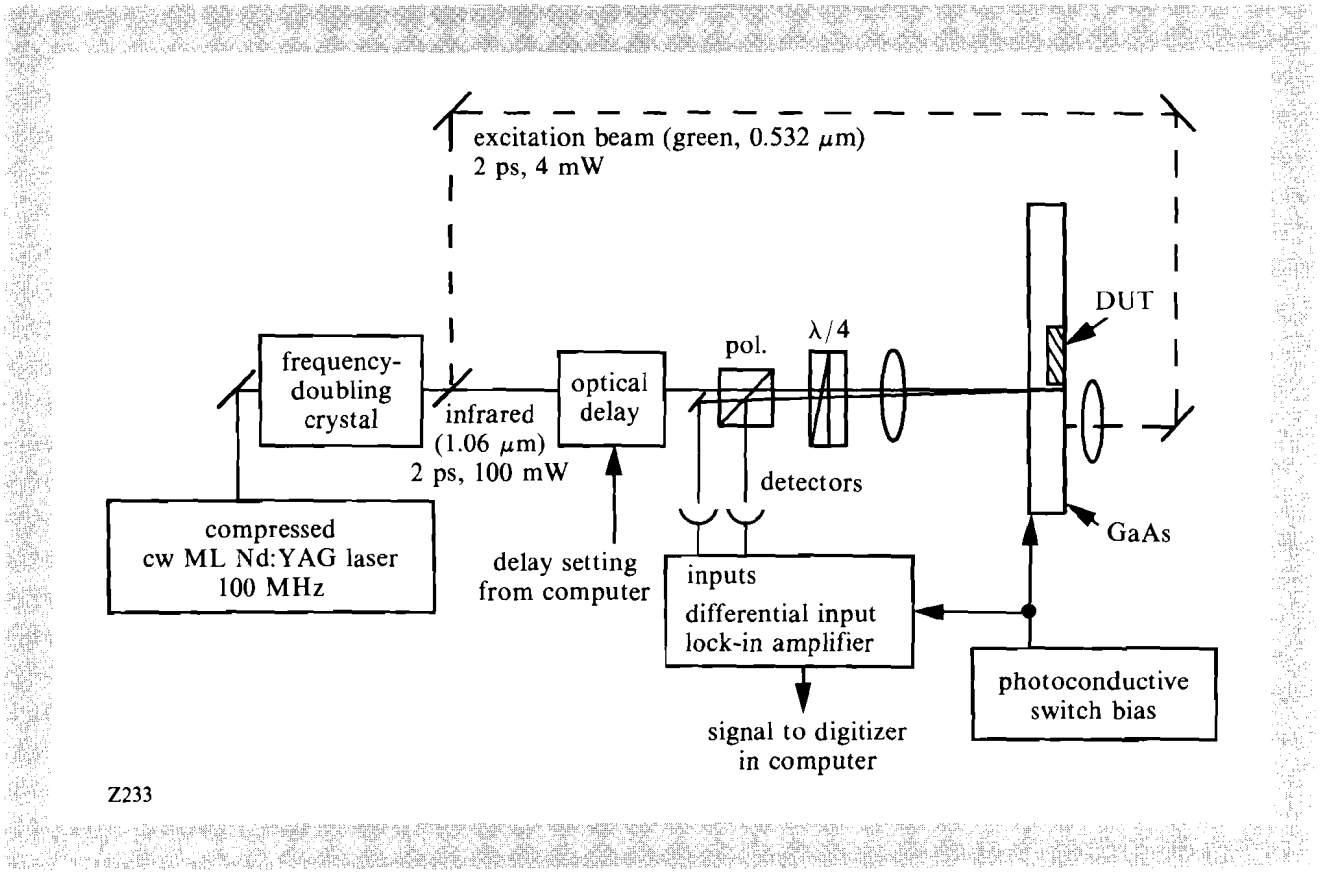

Fig. 32.10
Electro-optic sampling system.

Given the near-ideal nature of the electro-optic sampling, the major source of error in this approach was anticipated to be due to nonuniform waveguide characteristics. To test this, we acquired the waveforms from our experimental setup at a distance of 7 mm on each side of the switch. As can be seen in Fig. 32.11, good agreement in the wave shapes was observed until the reflection from point (a) occurs at approximately 120 ps.

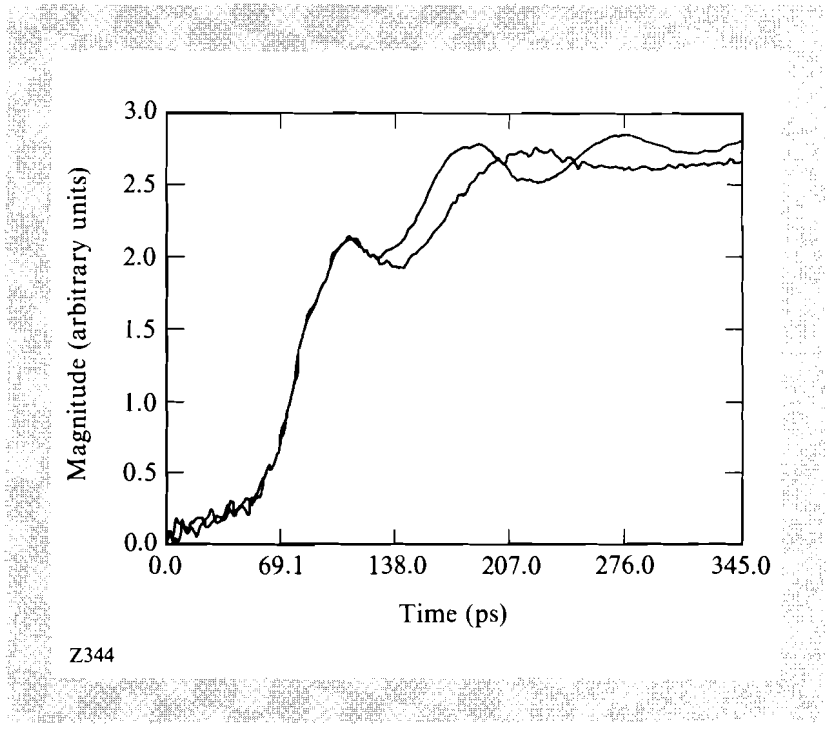

Fig. 32.11
Counterpropagating waveforms.

Essentially the same results were observed for an alternate implementation of the concept, using a 4-mm-long coplanar stripline consisting of two 50-μm-wide nickel-gold-germanium lines separated by 50 μm. The substrate was GaAs, and a 10-μm break in one line served as the photoconductive switch. Symmetrical waveforms with 4-ps rise times were obtained at a distance of 1.5 mm from the switch, demonstrating that symmetrical pulses with extremely high bandwidths may be obtained for high-frequency-device characterization.

These results indicate that waveguide propagation characteristics of sufficient uniformity for applying the counterpropagating-pulse approach to time-domain reflectometry are obtainable. In contrast to the conventional TDR, the potential advantages of a TDR based upon this approach can be enumerated as

1. Sampling is performed directly at the device/transmission line interface. As a result, de-embedding of the transmission line response is not required.

2. Device biasing may be applied on the end of the transmission line opposite the DUT, excluding wirebonds, if no circuit elements lie in the signal path. This feature allows waveform acquisition with a low degree of distortion. For GaAs devices,

transmission lines and the DUT may be fabricated on a common substrate, eliminating the need for wirebond connections.

3. Photoconductive switching and electro-optic sampling allow generation and acquisition of fast rise-time waveforms. Experiments may thus be conducted with signal bandwidths exceeding 100 GHz. The traveling-wave characterization of linear circuits, known as the scattering parameter method, can also conceivably be obtained from waveforms acquired with the symmetrical pulse propagation technique.

ACKNOWLEDGMENT

This work was supported by the United States Air Force Office of Scientific Research under contract F49620-87-C-0016 to the Ultrafast Optical Electronics Center at the Laboratory for Laser Energetics of the University of Rochester and by the Laser Fusion Feasibility Project at the Laboratory for Laser Energetics, which has the following sponsors: Empire State Electric Energy Research Corporation, General Electric Company, New York State Energy Research and Development Authority, Ontario Hydro, and the University of Rochester. Such support does not imply endorsement of the content by any of the above parties.

REFERENCES

1. J. A. Valdmanis, G. Mourou, and C. W. Gabel, *Appl. Phys. Lett.* **41**, 211–212 (1982).
2. J. A. Valdmanis and G. Mourou, *IEEE J. Quantum. Electron.* **QE-22**, 69–78 (1986).
3. J. A. Valdmanis, Ph.D. dissertation, The University of Rochester, 1983.
4. K. J. Weingarten *et al. Electron. Lett.* **21**, 765–766 (1985).
5. LLE Review **27**, 135–138 (1986).

2.C A Substrate-Independent Noncontact Electro-Optic Probe Using Total Internal Reflection

The process of designing high-speed integrated circuits requires a knowledge of the appropriate device responses within their range of operational frequencies. To answer this need for design information, several approaches have been used to sample ultrafast electrical transients. Of these approaches, only one, electro-optic sampling, gives the flexibility of noncontact probing while maintaining a 1-THz bandwidth. Two classes of a noncontact electro-optic sampling have been demonstrated to date:[1] one using an electro-optic device substrate as a probing medium, and a more versatile class, using an external electro-optic superstrate to sample fringe electric fields. Here we describe an embodiment of the second class.

Superstrate sampling first appeared in a paper entitled "Two-Dimensional E-Field Mapping of Picosecond Optics and Optoelectronics."[2] In this embodiment of electro-optic sampling, a slab

of electro-optic material is coated with a highly reflective dielectric stack and placed, reflective surface down, over an electronic circuit or device. A sampling beam then reflects off the coating, passing through electric fields fringing into the crystal above the device under test (DUT). Further improvement to this approach was made by trimming the electro-optic slab to a tip of 40- to 100-μm square to reduce dielectric loading.[3] This article presents a total-internal-reflection (TIR) electro-optic probe of small dimensions, which also eliminates the need for a high-reflectivity dielectric stack.

There are two main advantages attributed to the use of TIR in a probe tip. First, it eliminates the need for a dielectric stack, which must be at least 2-μm thick to prevent serious leakage of light through to the substrate. This improves the ultimate spatial resolution of the probe by allowing the tip to be brought within 1/5 λ of the surface being probed (λ is the probe beam wavelength) before TIR is frustrated and light is coupled into the DUT. Second, the probe is made more rugged by the removal of the dielectric stack.

A truncated pyramid, as illustrated in Fig. 32.12, is made to ~100-μm dimensions, with its walls at 22.5° to its axis. Light focused

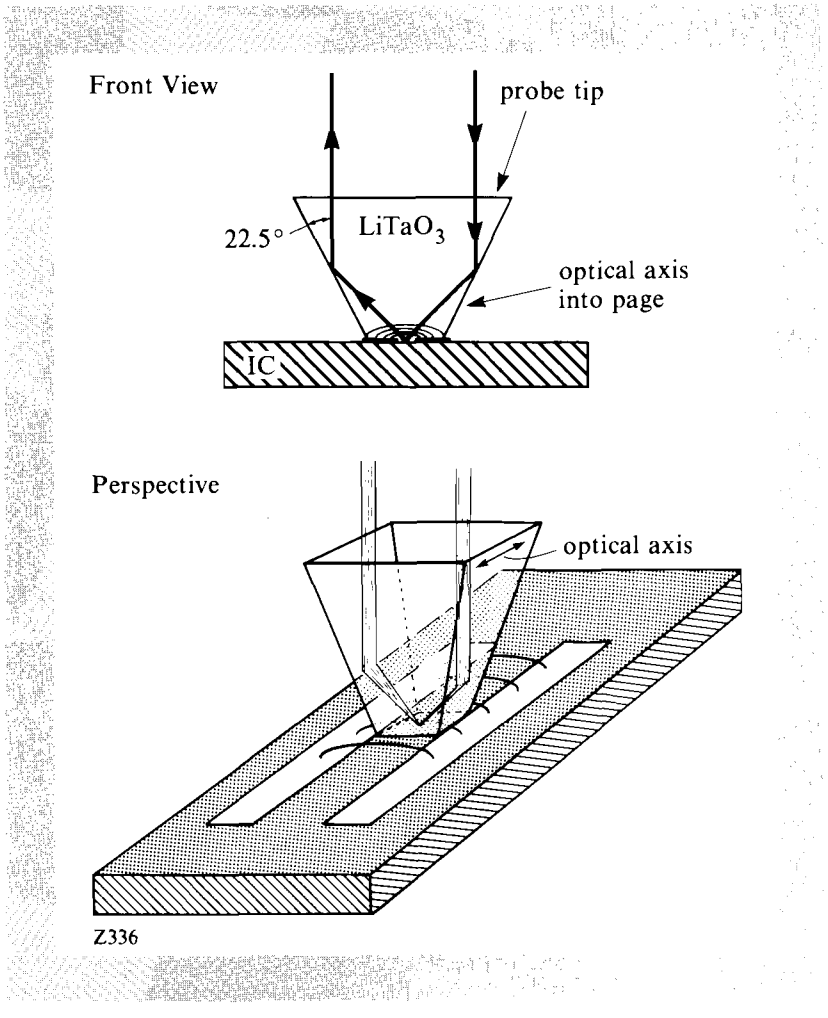

Fig. 32.12
Total internal reflection probe.

through the base of the probe may then reflect successively off a side wall, the probe tip, and the opposite wall, returning parallel to the input beam and displaced by twice the tip width. The alignment of the crystal's optical axis in this case would be normal to the plane of the beam; thus, it would sense components of electric field in that direction. A longitudinal "voltage" probe integrating $\mathbf{E}\cdot\mathbf{dz}$ along the optical axis could also be made using GaAs, KDP, or other crystals exhibiting a longitudinal Pockels effect. Once a TIR probe with a 100-μm square tip was fabricated, using standard polishing techniques, a system was configured as illustrated in Fig. 32.13 for testing a 1-μm-gate MESFET structure provided by Bell Northern Research. In this arrangement, a source laser having two beams of 70-fs pulses at a repetition rate of 100 MHz and an average power of about 2 mW is used both to trigger a test pulse and to sample electrical transients at appropriate points on the device. The trigger, or switching beam, passes through a variable optical delay line and is focused onto the gap between the device's gate and common source. This causes the gate to be momentarily switched to ground.

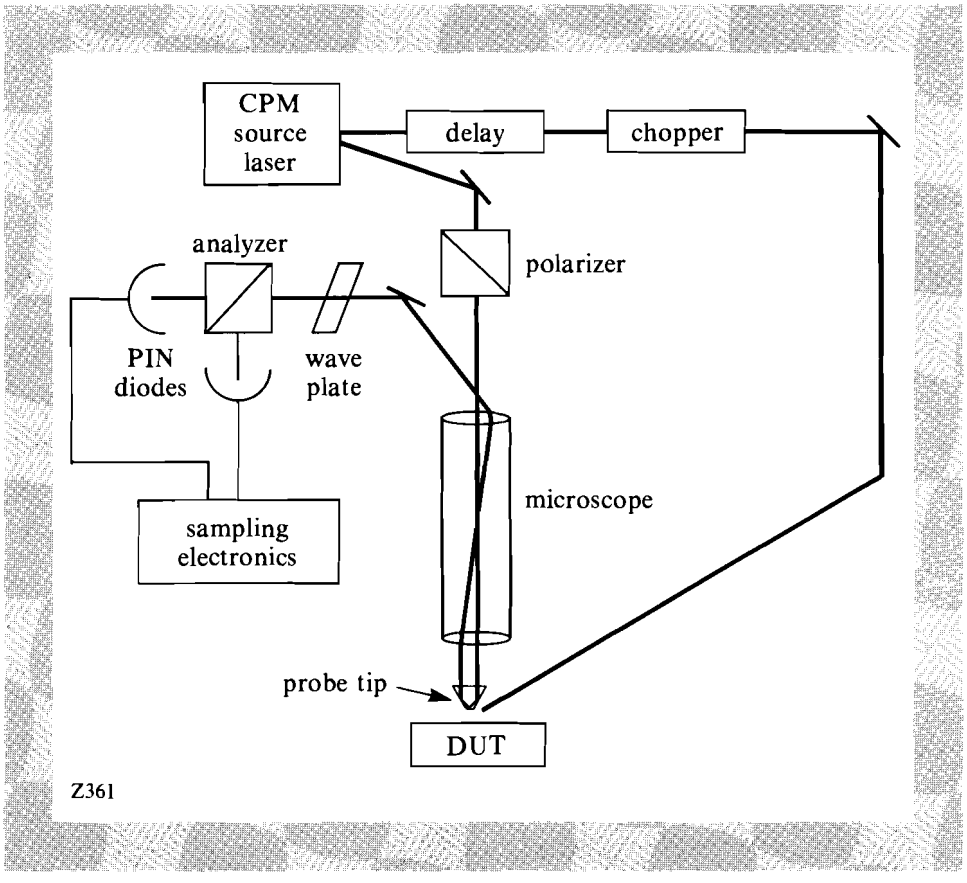

Fig. 32.13
Schematic of TIR probe in sampling system.

The second beam from the source laser, after passing through a polarizer oriented at 45° to the probe's optical axis, is focused onto the probe tip and then translated to the side, to retro-reflect through the probe as described previously. The probe beam then passes back through a compensator and analyzer and onto a pair of PIN photodiodes. A description of the sampling technique and signal processing used in this experiment can be found in Ref. 1.

Figure 32.14 shows the positions of the probe tip and excitation beam. The input signal was formed by optically exciting carriers in the 5-μm gap between the gate as source pads. With the TIR probe over the same gap, an input waveform was measured. Then, with the probe over the gap between source and drain pads, an output waveform was also measured. In either case, a known sinusoidal voltage was applied to the gaps to give a voltage calibration.

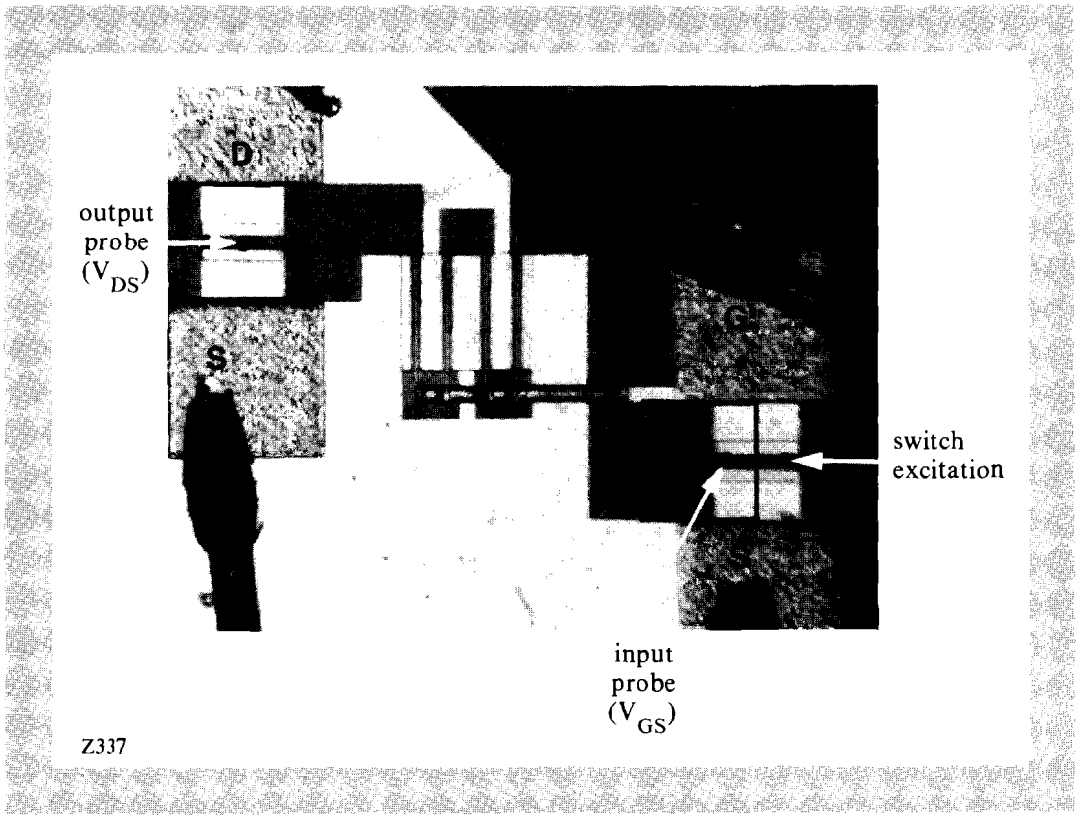

Fig. 32.14
1-μm gate MESFET tested using the TIR probe. The squares indicate probe positions; the circles indicate probe beam locations; and the fitted circle indicates the excitation beam position.

The 350-fs rise time of the input signal (Figs. 32.15 and 32.16) demonstrates the probe's ~1-THz bandwidth while the output (Fig. 32.17) indicates a 13-GHz device roll-off. The maximum device frequency corresponds to the value of f_{max} obtained using a standard network analyzer.

In conclusion, a rugged, noncontact, substrate-independent electro-optic probe with ~1-THz bandwidth has been demonstrated. Because this probe requires no dielectric coating, it provides the possibility of submicron spatial resolution. Work is currently in progress to use the bandwidth available with noncontact probes, to provide more standardized measurements for designers of ultrafast circuits.

ACKNOWLEDGMENT

This work was supported by the United States Air Force Office of Scientific Research under contract F49620-87-C-0016 to the Ultrafast Optical Electronics Center. At the Laboratory for Laser Energetics, additional support of laser facilities was provided through the Laser Fusion Feasibility Project, which has the following sponsors: Empire State Electric Energy Research Corporation, General Electric Company, New York State Energy Research and Development Authority, Ontario Hydro, and

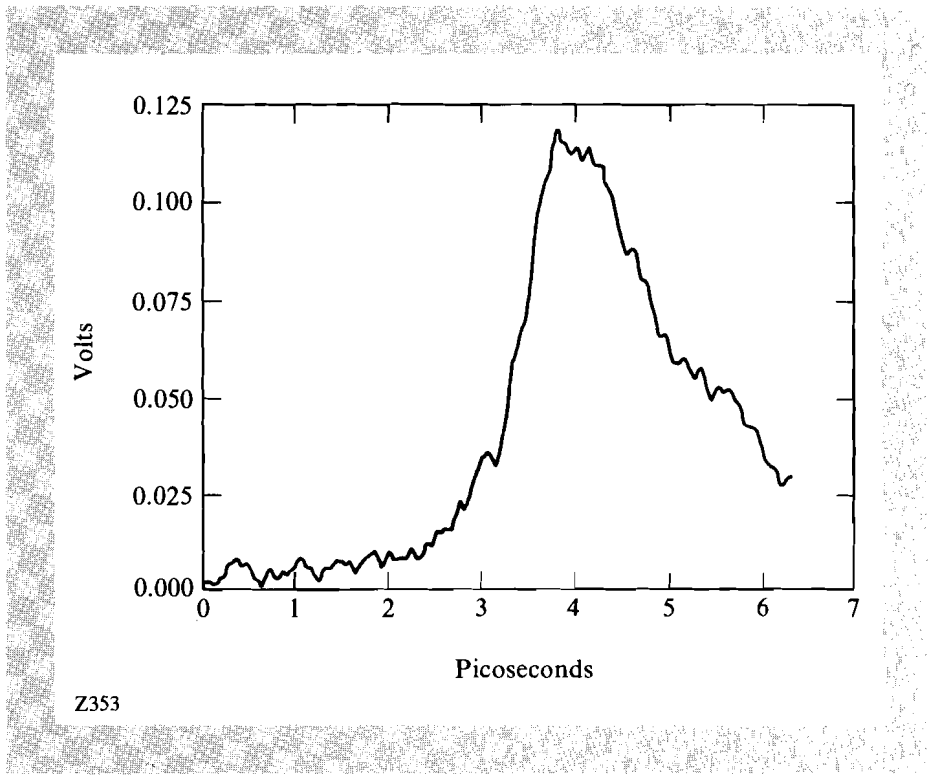

Fig. 32.15
Input electrical pulse showing the subpicosecond time response of the sampling system.

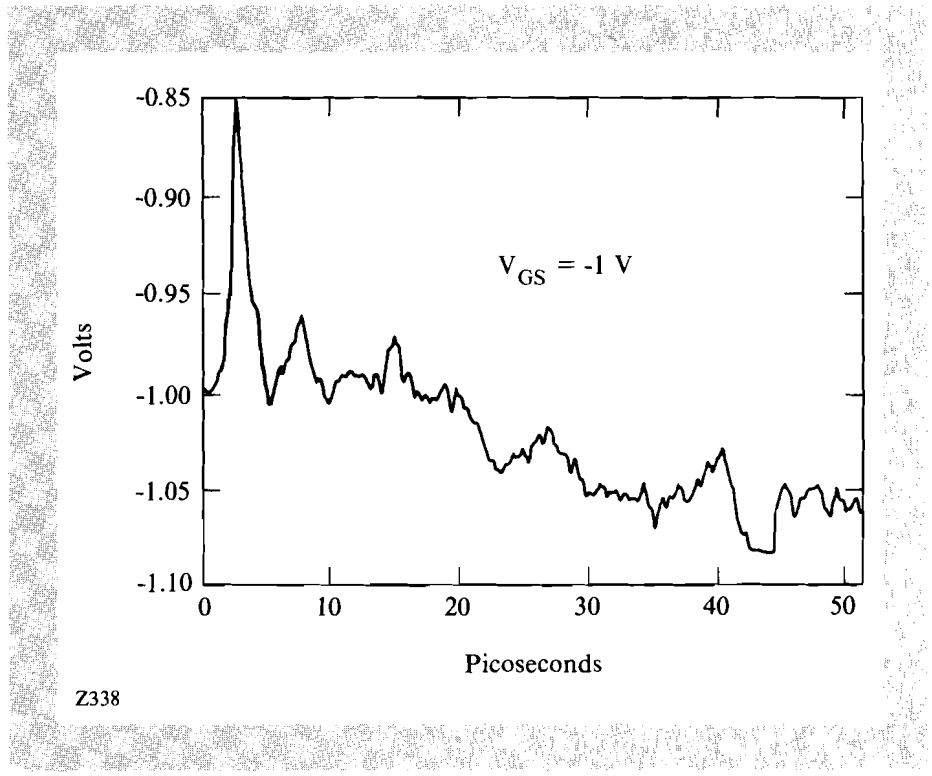

Fig. 32.16
Input waveform.

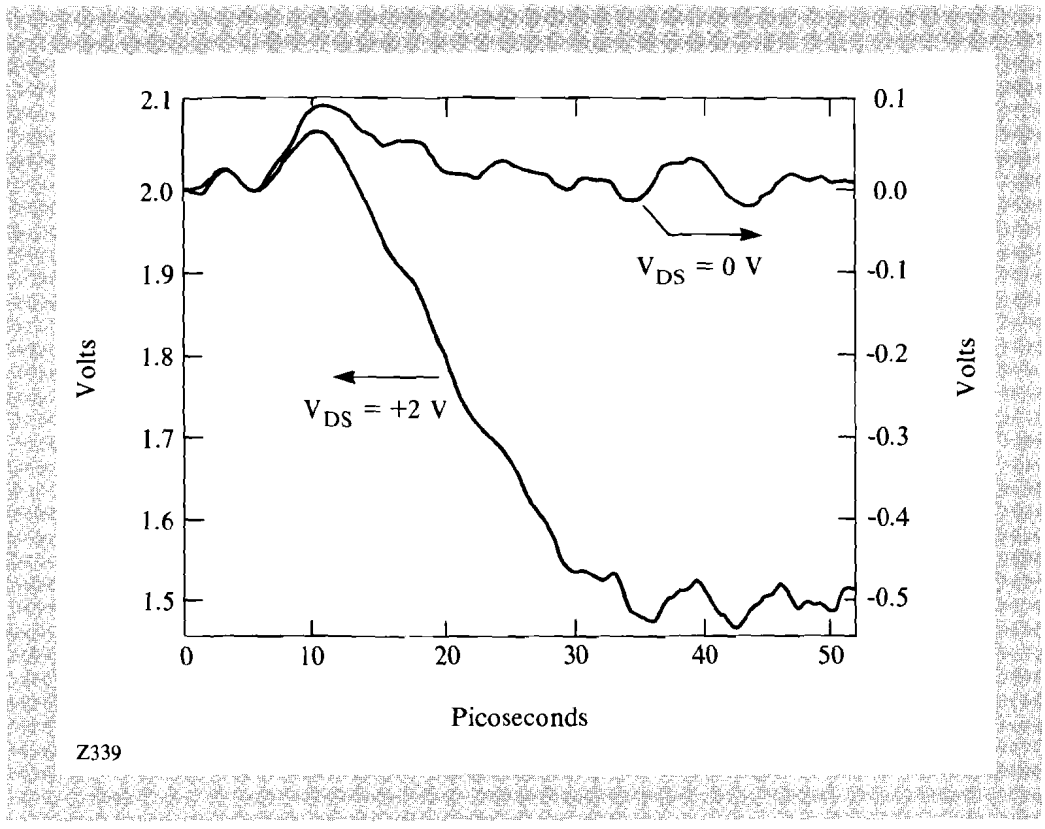

Fig. 32.17
Device output for biased and unbiased cases.

University of Rochester. Such support does not imply the endorsement of the content by any of the above parties.

The author wishes to thank Paul Jay and Bob Surridge at Bell Northern Research for providing the test structure.

REFERENCES

1. J. A. Valdmanis, G. A. Mourou, and C. W. Gabel, *Appl. Phys. Lett.* **41**, 211-212 (1982).

2. K. E. Meyer and G. A. Mourou, "Two-Dimensional E-Field Mapping with Subpicosecond Resolution," in *Picosecond Electronics and Optoelectronics*, edited by G. A. Mourou, D. M. Bloom, and C. H. Lee (Springer-Verlag, Berlin, 1985), pp. 54-57.

3. J. Nees and G. Mourou, *Electron. Lett.* **22**, 918-919 (1986).

2.D Picosecond-Reflection High-Energy Electron Diffraction

Pulsed-laser processing of semiconductors and metals is a rapidly growing field of study. Both the properties of the produced material (which could be unattainable by other means) and the fundamental processes are of great interest. Time-resolved observation of phenomena accompanying pulsed-laser processing has been accomplished by several different techniques. These include optical probing (both reflection and transmission),[1-5] photoconductivity measurement,[6] x-ray diffraction,[7] Raman scattering,[8] and time-of-flight mass spectrometry.[9] None of these techniques provides a surface structural probe that can be limited to the first few monolayers. Although second-harmonic generation could provide a surface structural probe,[10] its interpretation is ambiguous.[11]

Indeed, it is the properties of these initial atomic layers that are of prime importance in laser processing. In addition to its significance in device fabrication, the study of surface-phase transitions and reactions is a rapidly maturing science from both a theoretical and an experimental point of view. The advancement of such knowledge, however, requires the development of a direct time-resolved surface structural probe capable of monitoring the complex processes of surface-phase transitions and reactions. We report here on the demonstration of reflection high-energy electron diffraction (RHEED) with photogenerated picosecond electron pulses. Due to the synchronization of the electron pulses with the laser source, such a technique provides a picosecond time-resolved surface structural probe for material being irradiated with a laser.

Electron diffraction (both high energy and low energy) provides a "natural" surface probe that is well developed and has been used for decades in surface studies. Construction of a picosecond-transmission, electron-diffraction apparatus was accomplished a few years ago.[12] This technique was applied to study the dynamics of laser melting of freestanding thin-aluminum films.[13] Subsequently, a nanosecond, low-energy electron-diffraction apparatus was developed and used in surface temperature measurement during laser annealing of germanium.[14] In such a setup, due to the low electron energy, space-charge effects severely limited the ability to observe the diffraction pattern. It was estimated that on the average only one electron per shot was reflected from the surface.[14] Thus, averaging over a large number of shots was required to obtain meaningful data. This limitation precluded the use of this technique to study nonrecurring surface structural phenomena. In contrast, in picosecond RHEED, due to the much less severe space-charge limitations, we have demonstrated that excellent quality surface-diffraction patterns could be obtained with a total exposure time of the order of 100 ps.

The picosecond electron-diffraction system, shown in Fig. 32.18, was a modification of the previously described system.[12,13] The photocathode was ~250-Å gold film deposited on a sapphire window

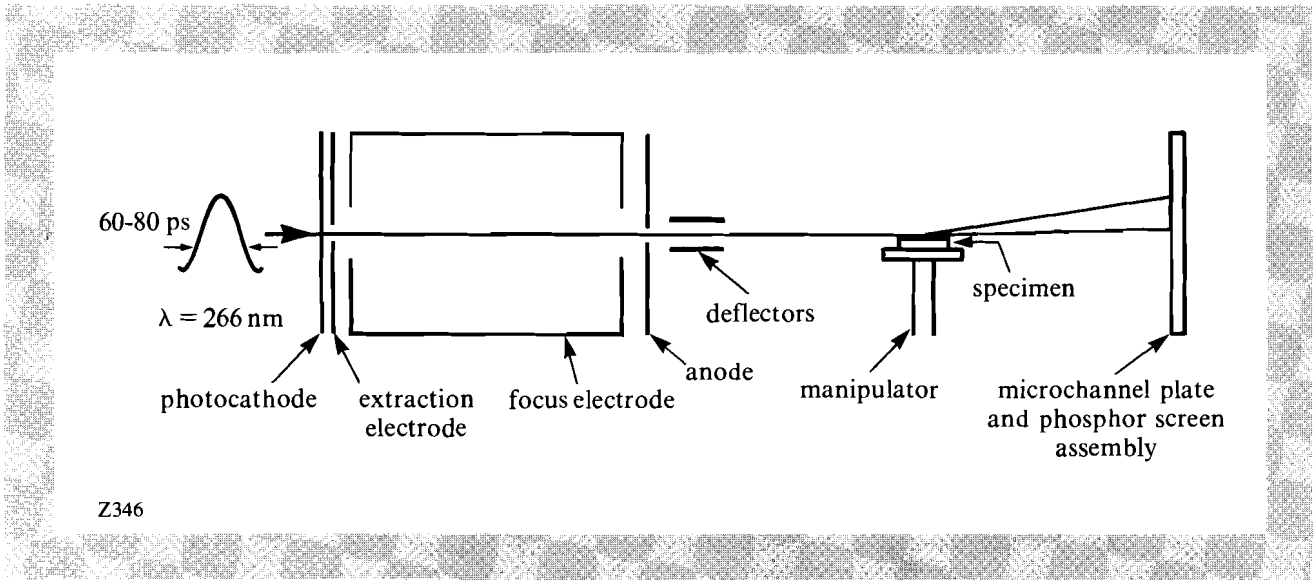

Fig. 32.18
A schematic diagram of picosecond time-resolved-reflection, high-energy electron-diffraction apparatus.

by conventional evaporation techniques. Such a photocathode was rugged enough to withstand months of operation with repeated exposure to the atmosphere. A circular aperture of 0.25-mm diameter located 1 mm from the photocathode was used as an extraction electrode, followed by a focus electrode and an anode that was located 140 mm from the photocathode. The specimen was mounted on a manipulator providing linear motion, rotation, and tilt. The diffraction pattern was amplified by a microchannel plate and observed using a P-47 phosphor screen deposited on a fiber optics faceplate, providing near-zero distortion of the diffraction pattern. The system was typically operated at a pressure of $\sim 2 \times 10^{-6}$ Torr.

The photocathode was activated by UV light from a frequency-quadrupled Nd:YAG regenerative amplifier (an injection-locked multipass amplifier[15]). This system provided 0.4-mJ pulses at 1.06 μm and a pulse width of 120 ps to 160 ps. The repetition rate of the regenerative amplifier could be varied from a single shot to 1.5 kHz with shot-to-shot stability better than 5%. Only a very small fraction of the output of the regenerative amplifier was frequency quadrupled ($< 10^{-3}$); thus, the 1.06-μm fundamental wavelength contained almost all the energy and could be used for sample heating. The frequency-quadrupled Nd:YAG ($\lambda = 0.266$ μm) was incident normal to the photocathode and had a ~ 0.1-mm spot-size diameter on it. The electron replica of the UV pulse, generated at the photocathode, was swept by the extraction aperture and further accelerated and focused in the focus electrode to a focal spot of ~ 0.8 mm on the phosphor screen. These electrons were incident in a grazing angle on the surface of the specimen and Bragg diffracted, giving a RHEED pattern.

Figure 32.19 shows a RHEED pattern of a cleaved surface of sodium chloride crystal obtained using a single-electron pulse and after averaging 50 pulses. The electron energy was 25 keV; a field of

Fig. 32.19
Reflection high-energy electron-diffraction patterns from a cleaved surface of a sodium chloride crystal: (a) using a single, ~200-ps electron pulse; (b) after averaging 50 pulses. The microchannel plate gain was reduced for (b).

23 kV/cm was applied between the photocathode and the extraction electrode. Although the number of electrons per pulse, measured by a Faraday cup and a picoammeter, was found to be directly proportional to the UV intensity on the photocathode, space-charge-induced temporal broadening of the electron pulse with increased UV intensity was observed. Measurements of the electron pulse width were accomplished by operating the diffraction system as a streak camera with the streak voltage supplied by a laser-activated Cr:GaAs photoconductive switch.[16,17] For conditions employed in Fig. 32.19, the electron pulse width used to obtain a RHEED pattern was measured at ~200 ps. The number of electrons delivered to the specimen per pulse was $\sim 5 \times 10^5$. As seen from Fig. 32.18(a), good RHEED patterns could be obtained with even a single electron pulse, making the study of nonrecurrent events possible. Better-quality diffraction patterns could be established by averaging several pulses, as shown in Fig. 32.18(b). Extension of the present technique to a few picosecond, or even subpicosecond, resolution should be possible by pulse compression of the driving laser and by minimization of electron temporal broadening.[18,19]

In summary, we have demonstrated the technique of picosecond time-resolved-reflection, high-energy electron diffraction. This technique represents a direct time-resolved surface structural probe limited to the first few monolayers and synchronized with the driving laser source. Application of this technique could include the study of surface structural and chemical changes. We are currently constructing a picosecond RHEED system operating in ultrahigh vacuum. Future experiments will include the study of surface phase transformations and chemical reactions.

ACKNOWLEDGMENT

This work was supported by the Office of Naval Research, contract No. N00014-85-K-0758, and the Air Force Office of Scientific Research, contract No. AFOSR-87-0327. Such support does not imply endorsement of the content by any of the above parties.

REFERENCES

1. J. M. Liu, H. Kurz, and N. Bloembergen, *Appl. Phys. Lett.* **41**, 643 (1982).
2. C. V. Shank, R. Yen, and C. Hirlimann, *Phys. Rev. Lett.* **50**, 454 (1983).
3. D. H. Lowndes, R. F. Wood, and R. D. Westbrook, *Appl. Phys. Lett.* **43**, 258 (1983).
4. M. C. Downer and C. V. Shank, *Phys. Rev. Lett.* **56**, 761 (1986).
5. H. E. Elsayed-Ali, T. B. Norris, M. A. Pessot, and G. A. Mourou, *Phys. Rev. Lett.* **58**, 1212 (1987).
6. P. S. Peercy, in *Laser Surface Treatment of Metals*, edited by C. W. Draper and P. Mazzoldi (Martinus Nijhoff Publishers, Dordrecht, 1986), p. 611.
7. B. C. Larson, J. Z. Tischler, and D. M. Mills, *J. Mater. Res.* **1**, 144 (1986).
8. D. von der Linde, G. Wartmann, and A. Compaan, *Appl. Phys. Lett.* **43**, 613 (1983).
9. A. Pospieszczyk, M. A. Harith, and B. Stritzker, *J. Appl. Phys.* **54**, 3176 (1983).
10. C. V. Shank, R. Yen, and C. Hirlimann, *Phys. Rev. Lett.* **51**, 900 (1983).
11. J. E. Sipe, V. Mizrahi, and G. I. Stegeman, *Phys. Rev. B* **35**, 9091 (1987).
12. G. Mourou and S. Williamson, *Appl. Phys. Lett.* **41**, 44 (1982).
13. S. Williamson, G. Mourou, and J. C. M. Li, *Phys. Rev. Lett.* **52**, 2364 (1984).
14. R. S. Becker, G. S. Higashi, and J. A. Golovchenko, *Phys. Rev. Lett.* **52**, 307 (1984).
15. I. N. Duling III, T. Norris, T. Sizer II, P. Bado, and G. A. Mourou, *J. Opt. Soc. Am. B* **2**, 616 (1985).
16. G. Mourou and W. Knox, *Appl. Phys. Lett.* **36**, 623 (1980).
17. G. Mourou, W. Knox, and S. Williamson, *Laser Focus* **18**, 97 (1982).
18. W. Sibbett, H. Niu, and M. R. Baggs, *Rev. Sci. Instrum.* **53**, 758 (1982).
19. K. Kinoshita, M. Ito, and Y. Suzuki, *Rev. Sci. Instrum.* **58**, 932 (1987).

2.E Radial Compression of Picosecond Electrical Pulses

Introduction

Acceleration of electrons and positrons in conventional rf linacs is presently limited to gradients of order 20 MV/m. To extend e^+e^- collisions to the TeV region, it is necessary to achieve gradients at least an order of magnitude larger, and several promising proposals are being explored.[1-3] The high electric field at the focus of intense lasers[4] provides a suitable gradient, but so far no practical geometry has been found for efficient particle acceleration.

Recently, Willis[5] suggested the use of ultrafast lasers to switch power from a DC high-voltage source onto an accelerating structure. The proposed structure consists of circular discs and thus acts as a radial transformer. If the rise time of the electrical pulse is of the order of the gap spacing (~ 1 mm), a voltage gain of a factor of 10 can be achieved. Furthermore, because of the small gap spacing a very high gradient is, in principle, attainable.

Radial compression of electrical pulses had been considered[6] in the 1960s and is used in accelerators such as the particle-beam fusion accelerator (PBFA);[7] recent studies on a large-scale model have been reported by Aronson *et al.*[8] A compact structure is needed for a high-energy accelerator; this has now become possible because of the availability of fast-pulsed lasers for driving the high-voltage switch. Willis and his group are working on laser-triggered photoemission from a wire cathode;[9] Villa[10] proposed a laser-triggered spark gap. Here we report on results obtained using photoconductive switching of high-resistivity silicon.

Using a high-power picosecond laser developed at LLE,[11] we were able to demonstrate voltage gain in a structure with an outer radius $R = 3$ cm and gap $g = 2$ mm. Since the field at the center of the disc must be measured with picosecond time resolution, we measured the electro-optic effect and sampled the waveform by delaying the optical probe.[10] A hard tube pulser provided the high voltage that was applied on the outer diameter of the discs 10 ns–100 ns before switching. The observed waveforms and their amplitude are in qualitative agreement with the calculated values.

Prototype Structure

The structure used in this investigation is shown in Fig. 32.20. The lower brass disk is grounded and the upper disc is a silicon wafer 500-μm thick. A gold coating on the inner side of the silicon serves as the "anode" to provide the conducting structure in which the pulse propagates. A ring of gold coating, connected to the high-voltage feed, was deposited on the other side of the silicon at its outer circumference. The two discs were separated by 2 mm and had a 1-mm-diameter hole at their center. A 2-mm-thick KDP crystal was placed at the center; it had dimensions 1×1 mm^2 and had a reflective coating on one side and it was probed in reflection.

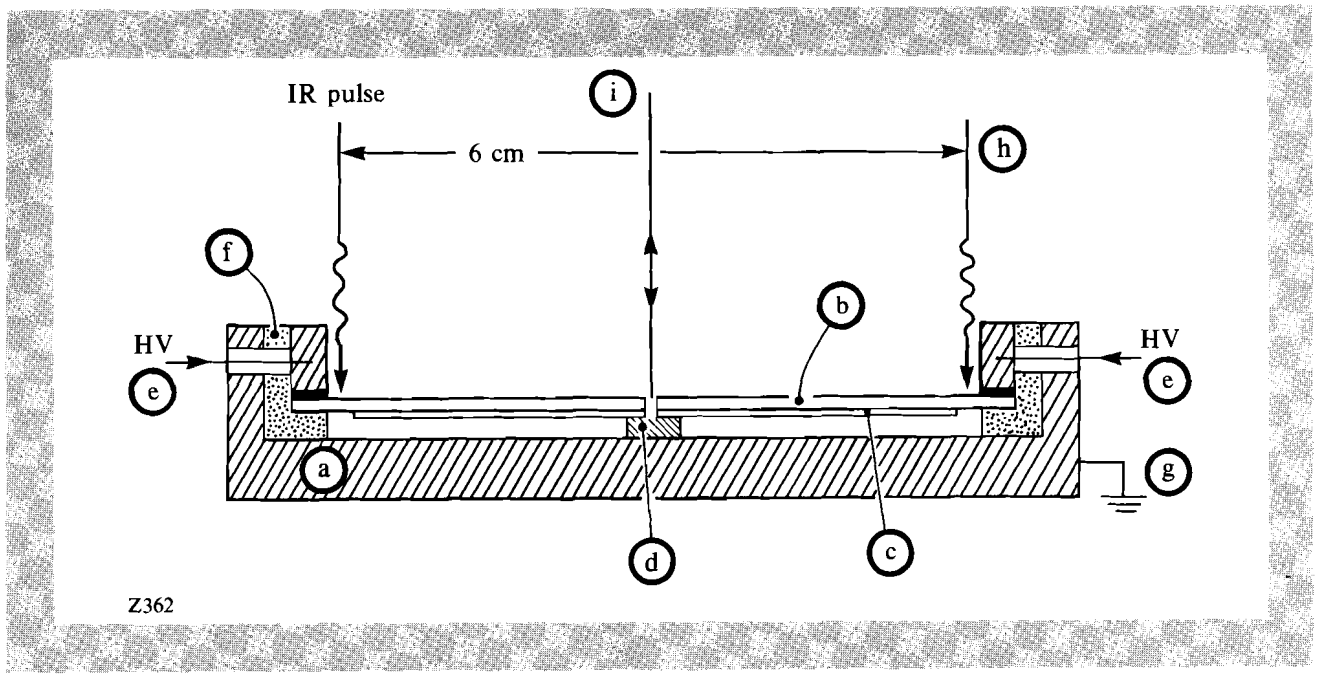

Fig. 32.20
Cross section of the disc structure: (a) cathode brass disc; (b) silicon wafer; (c) gold coating; (d) KDP crystal; (e) HV feed; (f) insulator; (g) ground; (h) IR pulse; and (i) probe pulse.

The equivalent electric circuit is shown in Fig. 32.21. The disc structure is represented by C2, even though at these speeds it is a distributed system; C1 is the charging capacity; C1 ~ 20 pF; and R1 represents the ohmic impedance across the silicon disc between the conducting coatings R1 ~ 10kΩ (ρ = 7kΩ-cm). S2 represents the photoconductive (ρ = 7kΩ-cm) switch, which shorts R1. When the charging pulse $-V_o$ is applied at C1, the upper plate of C2 floats toward $-V_o$, charging up C2; to prevent this, a small conducting spring, indicated by the inductance L1, was inserted between the discs.

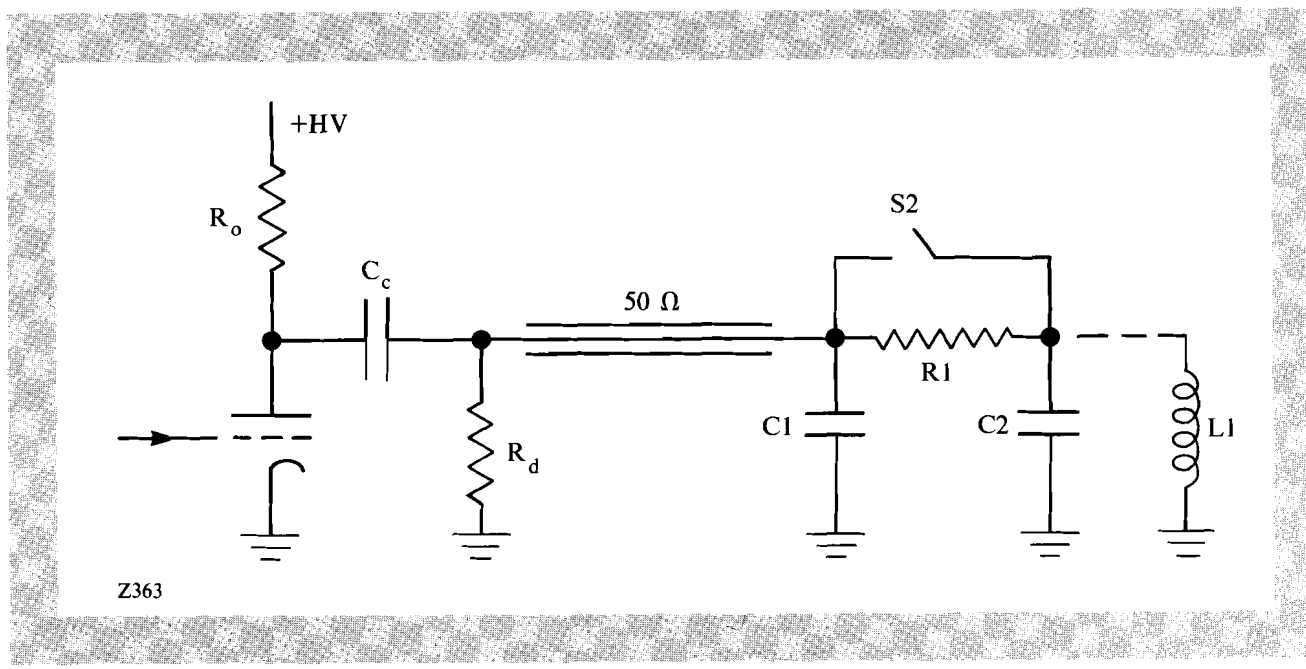

Fig. 32.21
The equivalent circuit for the structure.

The waveform at the charging electrode (i.e., the C1, R1 node) is shown in Fig. 32.22(a). Because of the impedance mismatch, the voltage builds up to $-V_o$ by successive reflections; the IR switching beam is blocked. Figure 32.22(b) shows the waveform when switching takes place by the IR pulse, whose timing is indicated on the lower trace.

The impedance seen by the electrical pulse that propagates between the two disks is a function of the radius r; it is given approximately by $Z(r) = (377\ \Omega)(g/2\pi r)$, with g the gap spacing. For constant power, the voltage squared is proportional to the impedance, so that a gain of order $V(r_o)/V_o = \sqrt{R/r_o}$, where r_o is the radius of the central aperture, can be expected. The propagation of a pulse of finite rise time can be calculated analytically,[10] obtaining for the voltage at the center of the discs

$$V_c = 2V_o\sqrt{\frac{2R}{g+c\tau_R}} \tag{1}$$

Here, V_o is the voltage at radius R and τ_R is the rise time of the pulse. Equation (1) shows the importance of ultrafast switching in maintaining a small gap between the discs.

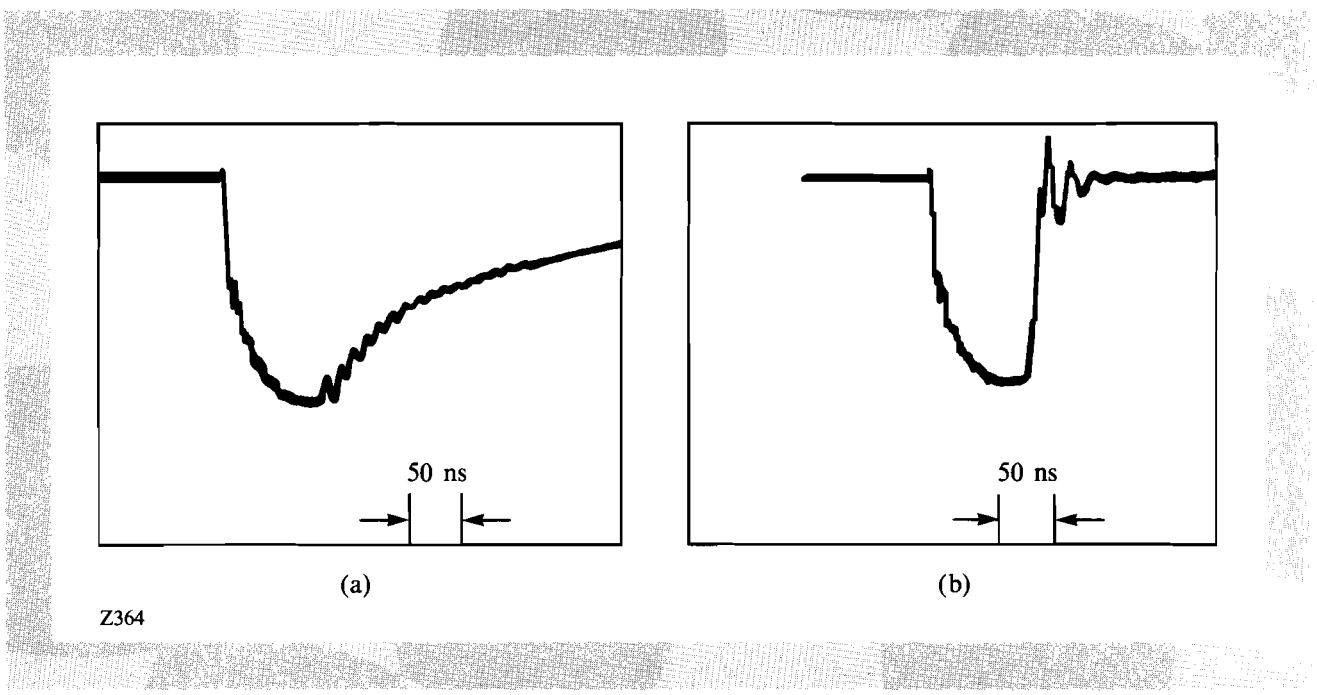

Fig. 32.22
The waveform at the HV feed point: (a) without switching, (b) with switching.

Optical System

The pulsed laser used in this investigation was a combination of a Nd:YLF oscillator and a Nd:glass amplifier ($\lambda = 1.054\ \mu m$), producing pulses of a few millijoules of 1-ps to 3-ps duration[11] at a repetition rate of 5 Hz. Pulses from a Nd:YLF mode-locked oscillator are stretched to 300 ps, chirped in a 1.5-km optical fiber, and injected into a regenerative amplifier. The pulse is amplified to saturation and

ejected from the optical cavity. The final pulse retains its chirp. Reflection gratings, arranged to compensate for the optical chirp, compress the pulse to 1 ps. This sequence is shown schematically in Fig. 32.23.

The spatial profile of the IR pulse was modified by an optical system incorporating a toroidal lens. The annulus of IR light was focused onto the silicon switch at the periphery of the radial transmission line. The attenuation length at $\lambda = 1.054$ μm is of the order of 1 mm, so that carriers are being produced throughout the bulk of the silicon wafer. A fraction of the pulse was split off, frequency doubled, and used to probe the electro-optic KDP crystal located at the center of the discs. A variable delay line in the pump beam provided the temporal scanning.

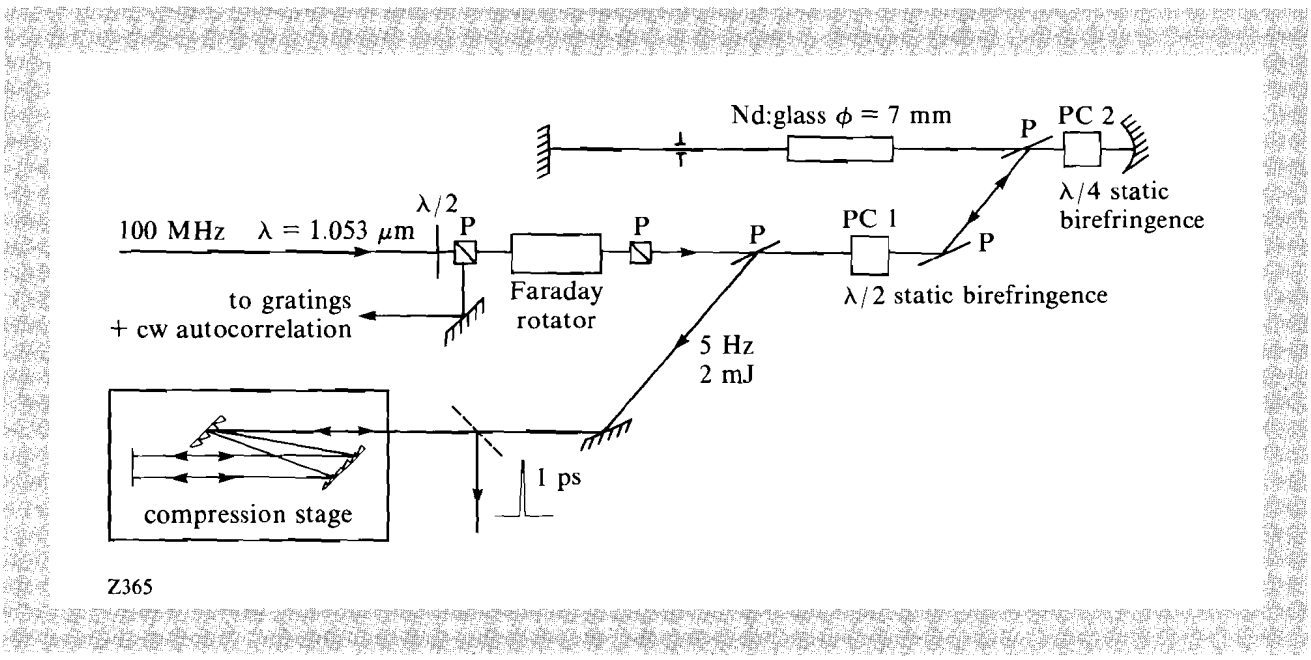

Fig. 32.23
Schematic of optical pulse amplification and compression.

The sampling system is shown schematically in Fig. 32.24. The frequency-doubled green beam is passed through a Glan-Thompson polarizer, followed by a compensator (variable retardation device), so that elliptically polarized light is incident on the electro-optic crystal. This crystal has the property that its birefringence changes in response to an applied electric field, thus changing the polarization of the light. After reflection, the beam retraces its path, and the component orthogonal to the original polarization direction is detected by a photodiode. The compensator is set so that after the double transversal the light is circularly polarized and the detector is biased to half of maximum intensity.

The electro-optic effect was longitudinal and thus independent of crystal thickness, yielding a half-wave voltage[12] $V_\pi = 10$ kV at $\lambda \sim 530$ nm. To improve signal to noise, the electrical pulse was applied on every second laser pulse, and the difference between 20 consecutive pulses was averaged in a boxcar integrator. Furthermore,

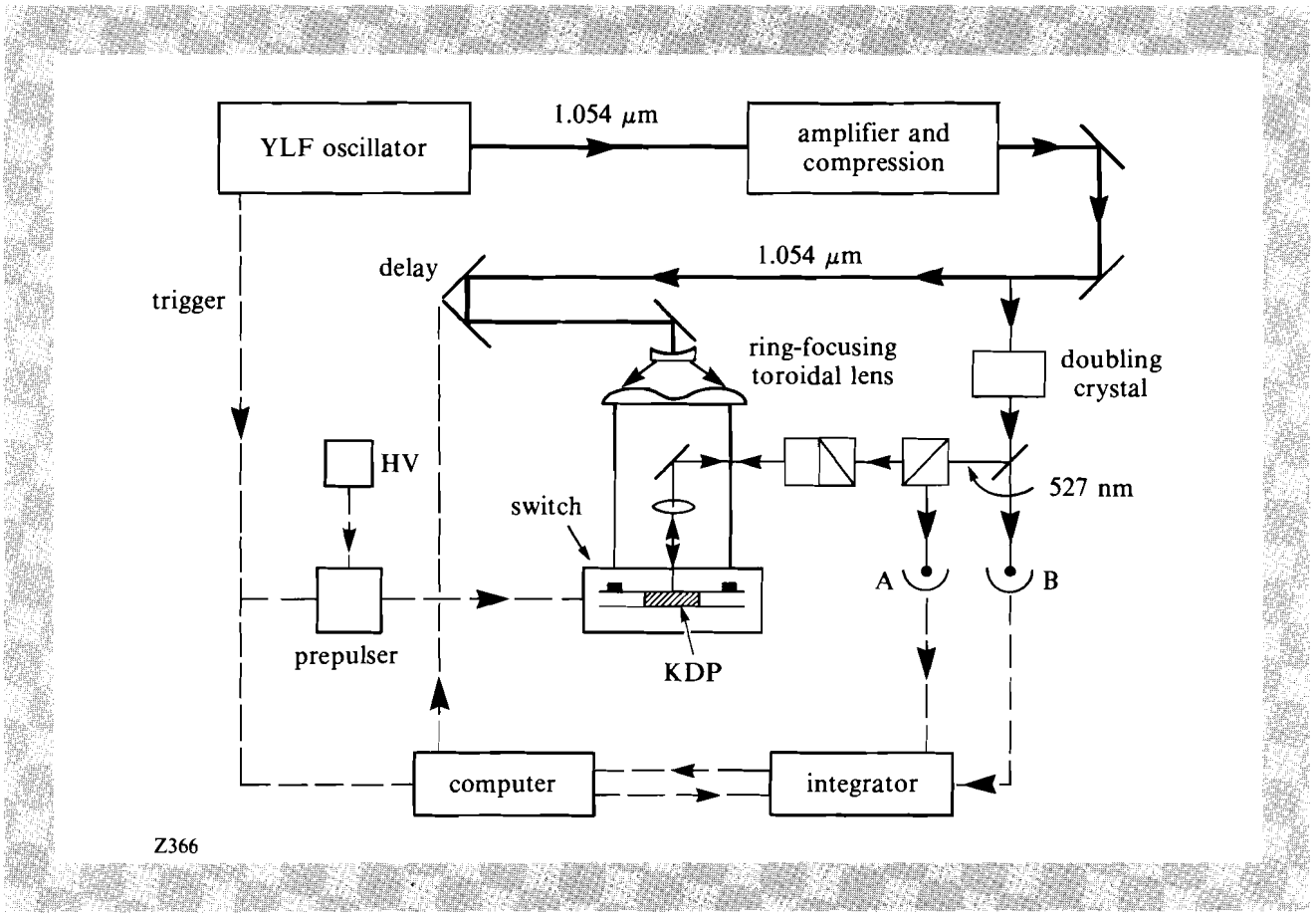

Fig. 32.24
Schematic arrangement of the electro-optic sampling.

the incident-pulse intensity was monitored and used for normalization. The output of the laser varies significantly from pulse to pulse, thus, it is necessary to use averaging techniques. The crystal was calibrated by applying a (quasi) static voltage (1.5 kV) across the discs. The results are shown in Fig. 32.25 and correspond to a bias ϕ = 0°, 45°, and 90°, respectively. At 45°, the rotation induced by the voltage pulse, which is applied for every second laser pulse, is clearly shown as a distinct trace. At 0° and 90°, the signal is quadratic in the optical rotation angle and beyond our resolution.

When fast switching is desired, it is important to prevent any type of prepulses from accompanying the main pulse. The prepulses bleed the voltage across the switch and can completely distort the rise time of the electrical pulse. Evidence for such prepulses can be seen in the trailing edge of the waveform of Fig. 32.22(b). The optical delay line had a travel of 9.4 cm and a step size of 6.25 μm. Data points were taken every 25 steps, or 1.04 ps. However, the time resolution of the system is set by the thickness of the crystal. Since the probe beam traverses the 2-mm-thick crystal twice, given a refractive index n = 1.5, the resolution is of the order of δt = 18 ps.

Results

In our first measurements, a Teflon insert ~1.5 cm in diameter was used to hold the crystal in the center of the discs. This insert produced

significant reflections and had to be removed. Distortions of the waveform were also seen in connection with prepulses; these were reduced by tuning the laser. The best waveform observed is shown in Fig. 32.26.

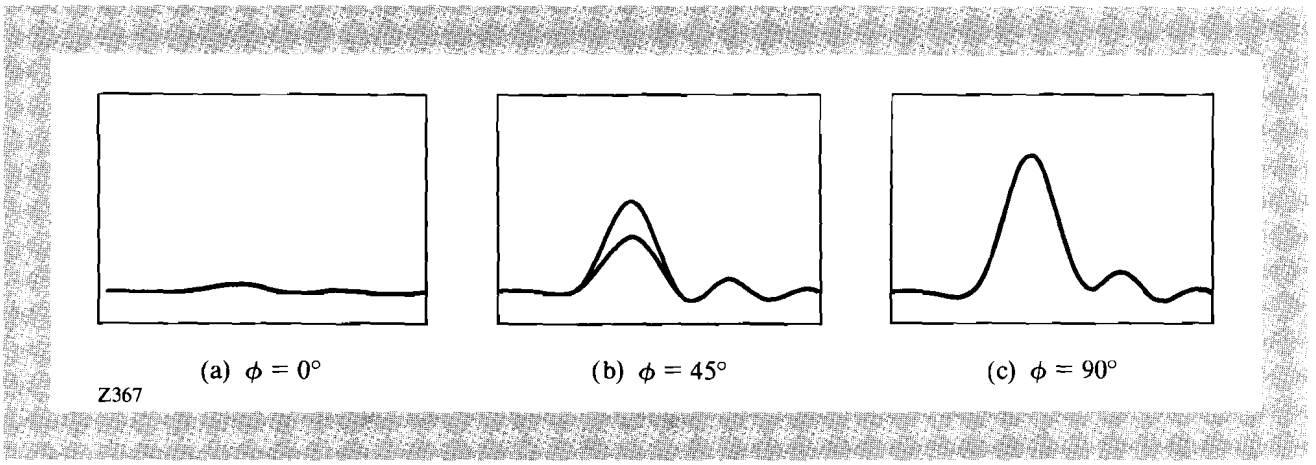

Fig. 32.25
Calibration of the electro-optic effect. The voltage is applied only for every second laser pulse. (a) Bias $\phi = 0°$; (b) bias $\phi = 45°$; (c) bias $\phi = 90°$. At $\phi = 45°$, the signal is proportional to Γ, the optical rotation; at $\phi = 0°$, $90°$ it is proportional to Γ^2 and therefore too small to be observed.

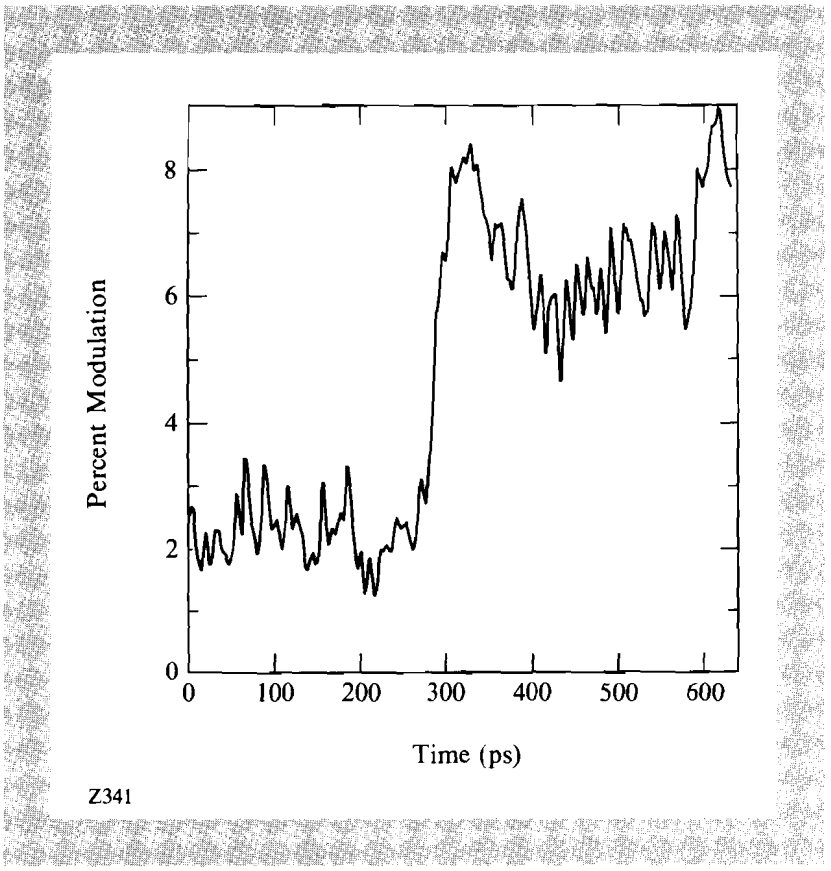

Fig. 32.26
The waveform observed at the center of the discs. The observed rise time is 24 ps but the resolution is 18 ps.

The measured rise time (10%–90%) is τ_M = 24 ps; this is a convolution of the actual rise time with the time resolution of the probe, δt = 18 ps. By simple quadrature, the true rise time is τ_R = 16 ps, and it is therefore probable that the peak amplitude exceeds the measured value by a factor of 1.5–2.0. A reflected pulse appears ~300 ps after the initial pulse. This corresponds roughly to the transit time for the round trip from the center of the disc to the edge of the structure and back (8 cm).

Based on the calibration of the crystal, the observed peak field is V_c = 1.0 kV. The charging voltage was V_o = 480 V, so that the observed gain is $V_c/V_o \sim 2$. To predict the gain from Eq. (1), we use τ_R = 16 ps, R = 3 cm, and g = 0.2 cm. The calculated gain is then

$$V_c = 2V_o\sqrt{8.8} = 5.9\ V_o\ . \tag{2}$$

Even if we take into account that (because of the resolution) the voltage at the center of the disc exceeds the observed V_c, the predicted value is greater than the observed value. This is probably due to reflections off the sampling crystal.

The propagation of the pulse on the structure has been calculated in detail by R. Barker, using a numerical integration code.[13] In that model, the silicon switch was closed with a 0.5-ps rise time and the measurements have not been smeared by finite resolution. The fields are calculated as a function of radius and time; Fig. 32.27 shows the waveform at the center. We note that in spite of the effects of

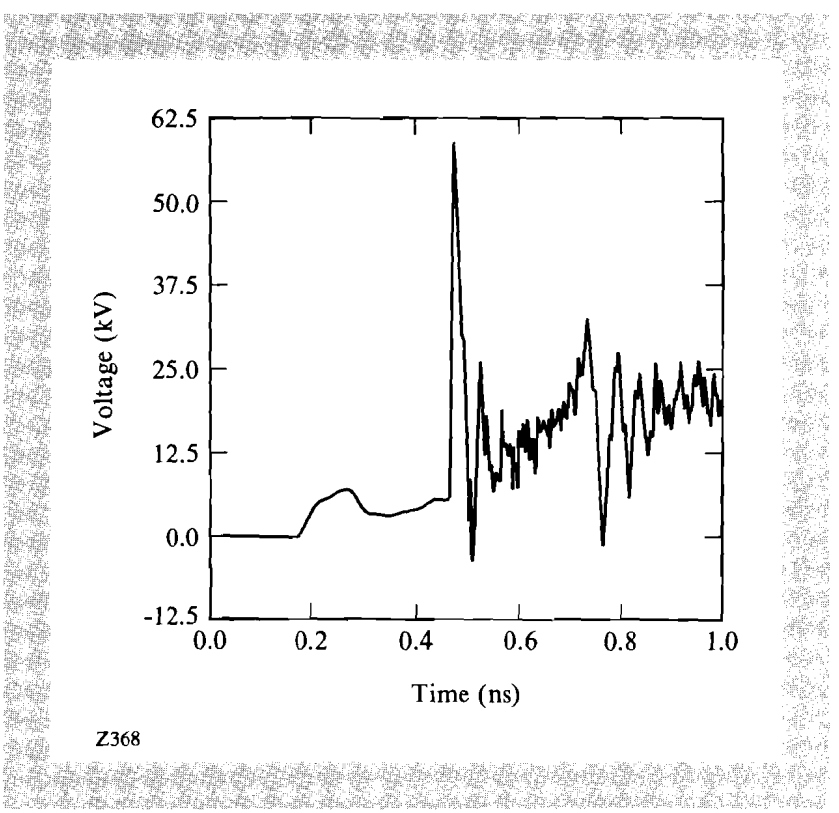

Fig. 32.27
The waveform at the center of the discs, as calculated in Ref. 13 for 0.5-ps rise time of the switch. Note the qualitative agreement with the observed data.

experimental resolution, the calculated waveform matches the observation very closely. The gain calculated by the numerical code is $V_c/V_o = 11$, in agreement with Eq. (1) for $\tau_R = 0$, $g = 1$ mm.

In conclusion, we have demonstrated that we can generate kilovolt electrical pulses with rise time $\tau_R = 16$ ps using a circular photoconductive switch. The propagation of this circular pulse toward the center gives rise to voltage gain in reasonable agreement with calculation. The energy in the switching pulse used for this investigation was ~ 1 mJ; we did, however, observe successful switching at significantly lower power levels as well.

Our present goal is to improve these measurements and observe gain of order ~ 10, while also increasing the supply voltage to a few tens of kV. We can then attempt to accelerate electrons photoemitted from the cathode; in that case, the KDP crystal is removed and the probe beam is frequency doubled once more so that the cathode is illuminated by a UV pulse. We believe that we can achieve gradients of 0.2 MV/mm–0.5 MV/mm and that one can stack several discs to make a structure of finite length. Such a device would make an electron source of high brilliance and could eventually be used for acceleration to TeV energies.

ACKNOWLEDGMENT

This work was supported by the U.S. Department of Energy Office of Inertial Fusion under agreement No. DE-FC08-85DP40200 and by the Laser Fusion Feasibility Project at the Laboratory for Laser Energetics, which has the following sponsors: Empire State Electric Energy Research Corporation, General Electric Company, New York State Energy Research and Development Authority, Ontario Hydro, and the University of Rochester. This work was also supported by the Air Force Office of Scientific Research grants AFOSR-84-017S and AFOSR-87-0328; by the U.S. Department of Energy under contract DE-AC02-76ER13065. Such support does not imply endorsement of the content by any of the above parties.

REFERENCES

1. A. M. Sessler and S. S. Yu, *Phys. Rev. Lett.* **58**, 2439 (1987).
2. T. Tajima and J. M. Dawson, *Phys. Rev. Lett.* **43**, 267 (1969).
3. G. A. Voss and T. Weiland, DESY Report 82-074 (1982); T. Weiland, *IEEE Trans. Nucl. Sci.* **NS32**, 3471 (1985).
4. K. Shimoda, *Appl. Opt.* **1**, 33 (1962).
5. W. Willis, "Switched-power Linac," CERN internal note EP/WJW/mm-0151D-1984.
6. E. C. Hartwig, "Pulsed line acceleration of electron rings," University of California preprint S/ERA-4, 1968.
7. See, for instance, B. N. Turman *et al., Proc. of the 5th IEEE Pulsed Power Conference* (IEEE, New York, 1985), p.155.
8. S. Aronson, F. Caspers, H. Haseroth, J. Knott, and W. Willis, paper presented at the Washington, DC, Acceleration Conference, March 1987.
9. T. Rao and J. Fisher, BNL Instrumentation Division (private communication).

10. R. E. Cassell and F. Villa, "Study of a high gradient pulsed linac structure," SLAC-PUB-3804 (October 1985); also F. Villa, "High gradient linac prototype: A modest proposal," SLAC-PUB-3875 (January 1986).

11. D. Strickland and G. Mourou, *Opt. Commun.* **55**, 447 (1985).

12. In reflection, the half-wave voltage is one half of the value given.

13. R. J. Barker (private communication). The code "MAGIC" was used.

Section 3
NATIONAL LASER USERS FACILITY NEWS

National Laser Users Facility (NLUF) activity during the fourth quarter of FY87 centered on a users' workshop and support of experiments on the OMEGA and glass development lasers (GDL).

On 14–15 July a workshop was held to familiarize more scientists with the facilities available at LLE. Representatives from industrial, government, and university laboratories were shown the current capabilities of the OMEGA and GDL lasers. User support available at LLE was outlined and the process of proposal submission and evaluation was explained. In addition, current users presented data from experiments done with the OMEGA and GDL lasers. The formal presentations were interspersed with discussion sessions to allow people new to LLE the opportunity to ask questions of the LLE staff and of current users.

Juan Marino and **Sam Goldsmith** from **Hans Griem**'s group at the University of Maryland conducted experiments on the OMEGA laser from 8 September through 14 September. Targets were manufactured and irradiated to study the propagation of the laser-initiated heat front into spherical targets. The primary diagnostics used were the NRL-NASA 3-m XUV spectrograph and the LBL SPEAXS time-resolved spectrograph. This data is now being analyzed at the University of Maryland.

A group of scientists from the University of California at Los Angeles, headed by **Prof. Chan Joshi**, conducted experiments on

GDL during the week of 14 September. Special targets were constructed at UCLA to study filamentation of high-intensity laser irradiation of flat targets. A combination of optical and x-ray diagnostics was used to measure laser-irradiated thin foils.

John Apruzese, **Philip Burkhalter**, and **John Seely** from Naval Research Laboratory (NRL) used both OMEGA and GDL to study the effect of collisional pumping with hot electrons on ionization states of tin and silver. GDL was propagated to the OMEGA target chamber in the infrared and used with ultraviolet irradiation from OMEGA to generate plasmas with and without hot electrons. Data were collected with x-ray crystal spectrographs, the NRL-NASA 3-m XUV spectrograph, x-ray imaging systems, and the SPEAXS time-resolved spectrograph. These measurements were conducted during the week of 21 September.

ACKNOWLEDGMENT

This work was supported by the U.S. Department of Energy Office of Inertial Fusion under agreement No. DE-FC08-85DP40200.

Section 4
LASER SYSTEM REPORT

4.A GDL Facility Report

The GDL system was an active target interaction facility for the entire period. Various experiments supported by GDL included x-ray conversion tests; preliminary studies for x-ray laser experiments; a number of shots to evaluate the benevolent smoothing effect of irradiating targets with laser beams that pass through ~200 Torr of inert gas, such as helium; several ALPHA backlighting experiments, where the GDL beam was transported to the OMEGA chamber; phase-plate tests; NLUF experiments; and other uniformity evaluations. The active mirrors are still being reworked in GDL; thus, system energies are currently limited to 200 J in the infrared.

A summary of GDL operations for this quarter follows:

Target Shots (BETA)	380
ALPHA Shots	8
Pointing Shots	78
Beamline Test Shots	80
TOTAL	546

4.B OMEGA Facility Report

During this period OMEGA served as a target irradiation facility for various experimental campaigns. There were no major upgrades on OMEGA in this quarter. Energies from the system remained reliably in the range of 1.5 kJ, with up to 1.9 kJ on demand. Beam-to-beam energy balance was as low as ±3%, with most shots in the ±5%-7% range. The predominant effort of the group was aimed at support of the high-density campaign.

In September, activities centered on the improvement of beam balance. A goal of ±3% is being sought, with a high-accuracy calibration of the MESS as the initial activity. New preamplifier packages have been installed on the MESS (multiwavelength emission-sensing system) "moose" calorimeters, improving their reliability. High-energy electrical calibrations were completed, as was tri-color calibration of the MESS diodes. User shots, for the University of Maryland, occupied a week of shooting OMEGA coincident with the ALPHA beam from GDL, in an experiment to test hot electron pumping of transitions in neon-like silver and tin. Accurate measurement of transport losses culminated the month's and fiscal year's activities, with final beam balances at 3.9% rms. Continued efforts will be spent to achieve the 3% goal.

A summary of OMEGA operations for this quarter follows:

Target Shots	299
Beamline Test Shots	129
Driver-Line Shots	71
TOTAL	499

As this report signals the end of the fiscal year, we note that the cumulative total of target shots with OMEGA (including ALPHA shots) this year was 814. This represents a increase of 36% over previous years, which can be attributed to the reliability of the OMEGA laser system, and to the hard work and dedication of the Operations Group.

ACKNOWLEDGMENT

This work was supported by the U.S. Department of Energy Office of Inertial Fusion under agreement No. DE-FC08-85DP40200, and by the Laser Fusion Feasibility Project at the Laboratory for Laser Energetics, which has the following sponsors: Empire State Electric Energy Research Corporation, General Electric Company, New York State Energy Research and Development Authority, Ontario Hydro, and the University of Rochester. Such support does not imply endorsement of the content by any of the above parties.

PUBLICATIONS AND CONFERENCE PRESENTATIONS

Publications

K. A. Cerqua, A. Lindquist, S. D. Jacobs, and J. Lambropoulos, "Strengthened Glass for High-Average-Power Laser Applications," *New Slab and Solid-State Laser Technologies and Applications* (SPIE, Bellingham, WA, 1987), Vol. 736, pp. 13–21.

H. E. Elsayed-Ali and G. A. Mourou, "Phase Transitions in the Picosecond Time Domain," *Interfaces, Superlattices, and Thin Films,* edited by J. D. Dow (Materials Research Society, Pittsburgh, PA, 1987), Vol. 77, pp. 51–57.

P. D. Goldstone, S. R. Goldman, W. C. Mead, J. A. Cobble, G. Stradling, R. H. Day, A. Hauer, M. C. Richardson, R. S. Marjoribanks, P. A. Jaanimagi, R. L. Keck, F. J. Marshall, W. Seka, O. Barnouin, B. Yaakobi, and S. A. Letzring, "Dynamics of High-Z Plasmas Produced by a Short-Wavelength Laser," *Phys. Rev. Lett.* **59,** 56–59 (1987).

H. Kim and M. D. Wittman, "X-Ray Microscopy of Inertial Fusion Targets Using a Laser-Produced Plasma as an X-Ray Source," *J. Vac. Sci. Technol. A* **5**, 2781–2784 (1987).

K. A. Cerqua, S. D. Jacobs, and A. Lindquist, "Ion-Exchange Strengthened Phosphate Laser Glass: Development and Applications," *J. Non-Cryst. Solids* **93**, 361–376 (1987).

S. M. Gracewski and R. Q. Gram, "Analysis of Forces on Inertial Confinement Fusion Targets During Ablation Layer Coating," *J. Vac. Sci. Technol. A* **5**, 2941–2944 (1987).

Forthcoming Publications

The following papers are to be published in the *Proceedings of the 17th Annual Boulder Damage Symposium*, Boulder, CO, October 1985:

K. A. Cerqua, S. D. Jacobs, B. L. McIntyre, and W. Zhong, "Ion Exchange Strengthening of Nd-Doped Phosphate Laser Glass."

B. Liao, D. J. Smith, and B. L. McIntyre, "The Development of Nodular Defects in Optical Coatings."

D. J. Smith, B. Krakauer, C. J. Hayden, A. W. Schmid, and M. J. Guardalben, "Yttrium-Oxide-Based Anti-Reflection Coating for High Power Lasers at 351 nm."

B. Yaakobi, "X-Ray Diagnostic Methods for Laser-Imploded Targets" and "Thermal Transport, Mass Ablation, and Preheat in Laser-Target Experiments," to be published in the *Proceedings of the Spring College on Radiation in Plasmas*, Trieste, Italy, June 1985 (World Scientific Publishing Co.).

G. Mourou, "Picosecond Electro-Optic Sampling," to be published in the *Proceedings of the High Speed Electronics Conference*, Stockholm, Sweden, August 1986.

W. R. Donaldson, "High-Speed, High-Repetition-Rate, High-Voltage Photoconductive Switching," to be published in the *Proceedings of the 2nd Topical Meeting on Picosecond Electronics and Optoelectronics*, Lake Tahoe, NV, January 1987.

G. Mourou, K. Meyer, J. Whitaker, M. Pessot, R. Grondin, and C. Caruso, "Ultrafast Optics Applied to Modern Device Research," to be published in the *Proceedings of the 2nd Topical Meeting on Picosecond Electronics and Optoelectronics*, Lake Tahoe, NV, January 1987.

R. W. Short, W. Seka, and R. Bahr, "Stimulated Raman Scattering in Self-Focused Light Filaments in Laser-Produced Plasmas," to be published in *Physics of Fluids*.

J. Delettrez, R. Epstein, M. C. Richardson, P. A. Jaanimagi, and B. L. Henke, "Effect of Laser Illumination Nonuniformity on the Analysis of Time-Resolved X-Ray Measurements in UV Spherical Transport Experiments," to be published in *Physical Review A*.

R. L. McCrory and J. M. Soures, "Inertially Confined Fusion," to be published in *Applications of Laser Plasmas*, Chapter 7.

K. A. Cerqua, J. Hayden, and W. C. LaCourse, "Stress Measurements in SOL-GEL Films," to be published in the *Journal of Non-Crystalline Solids*.

J. F. Whitaker, R. Sobolewski, D. R. Dykaar, T. Y. Hsiang, and G. A. Mourou, "Propagation Model for Ultrafast Signals on Superconducting Dispersive Striplines," to be published in a special issue of *IEEE Transactions on Microwave Theory and Techniques*.

T. Jackson, J. Nees, R. Vallee, and G. Mourou, "A Novel Method for Ultrahigh Frequency Electro-Optic Time-Domain Reflectometry," to be published in *Electronics Letters*.

T. Y. Hsiang, J. F. Whitaker, R. Sobolewski, D. R. Dykaar, and G. A. Mourou, "Propagation Characteristics of Picosecond Electrical Transients on Coplanar Striplines," to be published in *Applied Physics Letters*.

J. C. Lee, S. D. Jacobs, and A. Schmid, "Retro-Self-Focusing and Pinholing Effect in a Cholesteric Liquid Crystal," to be published in *Molecular Crystals and Liquid Crystals*.

S. Skupsky, "The 'Coulomb Logarithm' for Inverse Bremsstrahlung Laser Absorption," to be published in *Physical Review A*.

P. Maine, D. Strickland, P. Bado, M. Pessot, and G. Mourou, "Generation of Ultrahigh-Peak-Power Pulses by Chirped Pulse Amplification," to be published in the *IEEE Journal of Quantum Electronics*.

J. H. Kelly, D. L. Smith, J. C. Lee, S. D. Jacobs, D. J. Smith, J. C. Lambropoulos, and M. J. Shoup III, "A High-Repetition-Rate Cr:Nd:GSGG Active-Mirror Amplifier," to be published in *Optics Letters*.

W. Watson, "Vacuum-Assisted Contaminated Particulate Removal," to be published in the *Journal of Vacuum Science and Technology*.

A. Simon and R. W. Short, "Comments on 'Motion of an Electron Bunch Through a Plasma'," to be published in *Physics of Fluids*.

B. Yaakobi, "Recent Progress in X-Ray Laser Research," to be published in *Photonics*.

J. F. Whitaker, R. Sobolewski, D. R. Dykaar, T. Y. Hsiang, and G. A. Mourou, "Subpicosecond Pulse Propagation on Superconducting Striplines," to be published in the *Proceedings of the 18th International Conference on Low Temperature Physics*, Kyoto, Japan, August 1987.

H. E. Elsayed-Ali and G. A. Mourou, "Picosecond Reflection High-Energy Electron Diffraction," to be published in *Applied Physics Letters*.

The following papers are to be published in the *Proceedings of SPIE's 31st Annual International Technical Conference*, San Diego, CA, 16–21 August 1987:

P. A. Jaanimagi, J. Delettrez, G. G. Gregory, R. S. Marjoribanks, M. C. Richardson, D. K. Bradley, and B. L. Henke, "Application of X-Ray Streak Cameras for Fusion Diagnostics."

P. A. Jaanimagi, J. Duff, G. G. Gregory, R. L. Keck, M. C. Richardson, W. Seka, D. J. Bowley, S. Majumdar, and J. Wright, "Multi-Channel Optical Streak Cameras."

P. A. Jaanimagi, G. G. Gregory, S. A. Letzring, R. S. Marjoribanks, and M. C. Richardson, "Time-Resolved Grating Spectrograph Incorporating a Reflection Photocathode for Soft X-Ray Spectroscopy."

R. S. Marjoribanks, M. C. Richardson, P. R. Audebert, D. K. Bradley, G. G. Gregory, and P. A. Jaanimagi, "Time-Resolved Spectroscopy for Detailed Studies ($\lambda/\Delta\lambda > 1000$) of Weak X-Ray Emitters in Laser Plasmas."

G. G. Gregory, P. A. Jaanimagi, P. W. McKenty, S. A. Letzring, and M. C. Richardson, "Precision Alignment Techniques for Time-Resolved X-Ray Photography."

D. Shvarts, B. Yaakobi, P. Audebert, T. Boehly, B. Boswell, D. Bradley, R. S. Craxton, R. Epstein, M. C. Richardson, M. Russotto, and J. M. Soures, "Studies of New Geometries for X-Ray Laser Experiments."

T. Boehly, P. Audebert, D. Shvarts, B. Yaakobi, B. Boswell, D. Bradley, R. S. Craxton, R. Epstein, S. Noyes, M. C. Richardson, M. Russotto, and J. M. Soures, "Experimental Studies of New Geometries for X-Ray Laser Experiments."

P. Audebert, D. K. Bradley, M. C. Richardson, R. Epstein, P. A. Jaanimagi, O. Barnouin, J. Delettrez, B. Yaakobi, F. J. Marshall, and B. L. Henke, "Time- and Space-Resolved X-Ray Spectra of Imploding Laser Fusion Targets."

P. R. Audebert, O. Barnouin, J. Delettrez, R. Epstein, P. A. Jaanimagi, R. S. Marjoribanks, M. C. Richardson, and B. Yaakobi, "Space-Resolved High Resolution Spectroscopy of Laser Plasmas."

D. J. Smith, "Modeling of Nodular Defects in Thin Films for Various Deposition Techniques."

P. C. Cheng, H. Kim, and M. Wittman, "Microradiography with Laser-Produced Plasma Sources—Surface Roughness on PMMA Resist."

J. C. Lee, S. C. Jacobs, and R. J. Gingold, "Nd:YAG Laser with Cholesteric Liquid-Crystal Resonator Mirrors."

P. D. Goldstone, J. A. Cobble, A. Hauer, G. Stradling, W. C. Mead, S. R. Goldman, S. Coggeshall, M. C. Richardson, P. A. Jaanimagi, O. Barnouin, R. Marjoribanks, B. Yaakobi, F. J. Marshall, P. Audebert, and J. Knauer, "X-Ray Emission from High-Z Spherical Laser Plasmas: Implications for Plasma Dynamics."

J. F. Seely, U. Feldman, C. M. Brown, W. E. Behring, and M. C. Richardson, "High-Resolution XUV Spectroscopy Using the OMEGA Laser."

Conference Presentations

The following presentations were made at the 10th Korea Symposium on Science and Technology, Seoul, Korea, 7–18 July 1987:

H. Kim, "Recent Progress in Laser Fusion."

H. Kim, "Applications of Laser-Generated X-Ray Source."

K. A. Cerqua, J. E. Hayden, and W. C. LaCourse, "Stress Measurements in Sol-Gel Films," presented at the 4th International

Workshop on Glasses and Glass-Ceramics from Gels, Kyoto, Japan, 12–15 July 1987.

K. A. Cerqua, "Sol-Gel Processing of Materials," presented at Hoya Corporation, Research and Development Laboratories, Tokyo, Japan, July 1987.

J. S. Wark, "Short-Pulse X-Ray Diffraction from Laser-Shocked Crystals," presented at the APS Topical Conference on Shock Waves and Condensed Matter, Monterey, CA, July 1987 (invited).

The following presentations were made at SPIE's 31st Annual International Technical Conference, San Diego, CA, 16–21 August 1987:

P. A. Jaanimagi, J. Delettrez, G. G. Gregory, R. S. Marjoribanks, M. C. Richardson, D. K. Bradley, and B. L. Henke, "Application of X-Ray Streak Cameras for Fusion Diagnostics."

P. A. Jaanimagi, J. Duff, G. G. Gregory, R. L. Keck, M. C. Richardson, W. Seka, D. J. Bowley, S. Majumdar, and J. Wright, "Multi-Channel Optical Streak Cameras."

P. A. Jaanimagi, G. G. Gregory, S. A. Letzring, R. S. Marjoribanks, and M. C. Richardson, "Time-Resolved Grating Spectrograph Incorporating a Reflection Photocathode for Soft X-Ray Spectroscopy."

R. S. Marjoribanks, M. C. Richardson, P. R. Audebert, D. K. Bradley, G. G. Gregory, and P. A. Jaanimagi, "Time-Resolved Spectroscopy for Detailed Studies ($\lambda/\Delta\lambda > 1000$) of Weak X-Ray Emitters in Laser Plasmas."

G. G. Gregory, P. A. Jaanimagi, P. W. McKenty, S. A. Letzring, and M. C. Richardson, "Precision Alignment Techniques for Time-Resolved X-Ray Photography."

D. Shvarts, B. Yaakobi, P. Audebert, T. Boehly, B. Boswell, D. Bradley, R. S. Craxton, R. Epstein, M. C. Richardson, M. Russotto, and J. M. Soures, "Studies of New Geometries for X-Ray Laser Experiments."

T. Boehly, P. Audebert, D. Shvarts, B. Yaakobi, B. Boswell, D. Bradley, R. S. Craxton, R. Epstein, S. Noyes, M. C. Richardson, M. Russotto, and J. M. Soures, "Experimental Studies of New Geometries for X-Ray Laser Experiments."

P. Audebert, D. K. Bradley, M. C. Richardson, R. Epstein, P. A. Jaanimagi, O. Barnouin, J. Delettrez, B. Yaakobi, F. J. Marshall, and B. L. Henke, "Time- and Space-Resolved X-Ray Spectra of Imploding Laser Fusion Targets."

P. R. Audebert, O. Barnouin, J. Delettrez, R. Epstein, P. A. Jaanimagi, R. S. Marjoribanks, M. C. Richardson, and B. Yaakobi, "Space-Resolved High Resolution Spectroscopy of Laser Plasmas."

D. J. Smith, "Modeling of Nodular Defects in Thin Films for Various Deposition Techniques."

P. C. Cheng, H. Kim, and M. Wittman, "Microradiography with Laser-Produced Plasma Sources – Surface Roughness on PMMA Resist."

J. C. Lee, S. C. Jacobs, and R. J. Gingold, "Nd:YAG Laser with Cholesteric Liquid-Crystal Resonator Mirrors."

P. D. Goldstone, J. A. Cobble, A. Hauer, G. Stradling, W. C. Mead, S. R. Goldman, S. Coggeshall, M. C. Richardson, P. A. Jaanimagi, O. Barnouin, R. Marjoribanks, B. Yaakobi, F. J. Marshall, P. Audebert, and J. Knauer, "X-Ray Emission from High-Z Spherical Laser Plasmas: Implications for Plasma Dynamics."

J. F. Seely, U. Feldman, C. M. Brown, W. E. Behring, and M. C. Richardson, "High-Resolution XUV Spectroscopy Using the OMEGA Laser."

J. F. Whitaker, R. Sobolewski, D. R. Dykaar, T. Y. Hsiang, and G. A. Mourou, "Subpicosecond Pulse Propagation on Superconducting Striplines," presented at the 18th International Conference on Low Temperature Physics, Kyoto, Japan, 20–26 August 1987.

R. Sobolewski, J. F. Whitaker, D. R. Dykaar, T. Y. Hsiang, and G. A. Mourou, "Dispersion in Superconducting Transmission Lines," presented at the International Superconductivity Electronics Conference, Tokyo, Japan, 28–29 August 1987.

ACKNOWLEDGMENT

The work described in this volume includes current research at the Laboratory for Laser Energetics, which is supported by Empire State Electric Energy Research Corporation, General Electric Company, New York State Energy Research and Development Authority, Ontario Hydro, the University of Rochester, and the U.S. Department of Energy Office of Inertial Fusion under agreement No. DE-FC08-85DP40200.